Theor Chem Acc (2012) 131:1127
DOI 10.1007/s00214-012-1127-9

REGULAR ARTICLE

Telluroformaldehyde and its derivatives: structures, ionization potentials, electron affinities and singlet–triplet gaps of the X_2CTe and XYCTe (X,Y = H, F, Cl, Br, I and CN) species

Naziah B. Jaufeerally · Hassan H. Abdallah · Ponnadurai Ramasami · Henry F. Schaefer III

Received: 1 April 2011 / Accepted: 6 August 2011 / Published online: 10 March 2012

Abstract A systematic investigation of the X_2CTe and XYCTe (X,Y = H, F, Cl, Br, I and CN) species is carried out using the second-order Møller–Plesset perturbation theory and density functional theory. The basis sets used for all atoms (except iodine and tellurium) in this work are of double-ζ plus polarization quality with additional *s*- and *p*-type diffuse functions and denoted DZP++. The LANL2DZdp ECP and 6-311G(*d*,*p*) basis sets are used for tellurium and iodine. Vibrational frequency analyses are performed to evaluate zero-point energy corrections and to determine the nature of the stationary points located. The ionization potentials (IP_{ad} and $IP_{ad(ZPVE)}$), the four different forms of neutral–anion separations (EA_{ad}, $EA_{ad(ZPVE)}$, VEA and VDE), the singlet–triplet splittings as well as the HOMO–LUMO gaps are predicted. The electronegativity (χ) reactivity descriptor for the halogens (F, Cl, Br and I) and the calculated Mulliken's electronegativity are used as tools to assess the interrelated properties of these telluroformaldehyde derivatives. The predicted $IP_{ad(ZPVE)}$ values with the B3LYP functional range from 7.89 [I_2CTe] to 9.16 eV [F(NC)CTe], the $EA_{ad(ZPVE)}$ ranges from 1.29 [I_2CTe] to 3.34 eV [$(NC)_2CTe$], the singlet–triplet splitting ranges from 0.64 [H(NC)CTe)] to 1.85 eV [F_2CTe], and the HOMO–LUMO gap ranges from 2.21 [H(NC)CTe] to 3.42 eV [F_2CTe]. The HOMO–LUMO gap is found to be proportional to the singlet–triplet splitting. The results obtained are critically analyzed and discussed. This research is also compared with analogous studies of formaldehyde, thioformaldehyde and selenoformadehyde.

Keywords Telluroformaldehyde · Ionization potential · Electron affinity · Singlet-Triplet gap · HOMO-LUMO gap

1 Introduction

The physicochemical and spectroscopic properties of the XYCZ molecular series (X,Y = H, F, Cl and Br; Z = O, S and Se) have been the subject of various theoretical studies [1–4], aiming to help in the identification of these species for which experimental data are still elusive. Knowledge of the properties of these molecules is important for a better understanding of both the chalcogen effect and the halogenosubstitution effect in chemistry and biochemistry [1, 4].

The X_2CO (X = F or Cl) carbonyl halides have been found to be major products of the photolysis of halomethanes in the presence of oxygen [5], and the existence of F_2CO and Cl_2CO in the stratosphere has been confirmed [6]. Kwiatkowski and Leszczyski [1] used ab initio HF and the MP2 levels of theory with triple-ζ valence shell basis sets to predict the molecular parameters and the vibrational IR spectra of X_2CO (X = H, F, Cl and Br), which might be useful in the

Dedicated to Professor Eluvathingal Jemmis and published as part of the special collection of articles celebrating his 60th birthday.

Electronic supplementary material The online version of this article (doi:10.1007/s00214-012-1127-9) contains supplementary material, which is available to authorized users.

N. B. Jaufeerally · P. Ramasami (✉)
Computational Chemistry Group, Department of Chemistry, University of Mauritius, Réduit, Mauritius
e-mail: ramchemi@intnet.mu

H. H. Abdallah
School of Chemical Sciences, Universiti Sains Malaysia, 11800 Penang, Malaysia

H. F. Schaefer III (✉)
Center for Computational Quantum Chemistry, University of Georgia, Athens, GA 30602, USA
e-mail: fri@uga.edu

understanding of these species in stratospheric photooxidation. The energetics of formaldehyde have been extensively studied over the past years [7–10]. The ionization potential of formaldehyde (10.88 eV) was determined by Ohno et al. [9], using Penning ionization electron spectroscopy. The electron affinity of H_2CO (−0.65 eV) obtained using electron transmission spectroscopy was reported by Burrow and Michejda [7]. The adiabatic electron affinity (−0.96 eV) and the adiabatic ionization potential (10.82 eV) of formaldehyde were reported by Francisco and Thoman [10], at the CCSD(T)/6-311++G(3df,3pd) level of theory. Lai et al. [11] used the B3LYP/6-311G(*d*) method to calculate the HOMO–LUMO gap (6.13 eV) of formaldehyde.

Thioformaldehyde is the prototype molecule for the thiocarbonyl series. Thioformaldehyde has been extensively studied, both experimentally and theoretically [2, 10–22]. The ionization potential of thioformaldehyde from the electron impact measurements is reported to be 9.44 eV [19], while Rauk et al. [20] used post-Hartree–Fock methods with the 6-31G basis set to compute the adiabatic ionization energy (9.08 eV). Staneke [21] used Fourier transform ion cyclotron resonance (FT–ICR) mass spectrometry to measure the electron affinity of thioformaldehyde (0.47 eV) and See-Wing et al. [22] used the MP2/6-31G(*d*) level of theory to calculate the adiabatic electron affinity (0.38 eV). Lai et al. [11] used the B3LYP/6-311G(*d*) method to report the HOMO–LUMO gap of thioformaldehyde as 3.78 eV. The thio analogues of the nucleic acid bases and their ribose derivatives are among the most active antimetabolites [23], and some of these are known to exhibit activity against certain types of tumors [24]. Careless et al. [25] used microwave spectroscopy to report the molecular parameters of thiocarbonyl fluoride, F_2CS. The average molecular structure of Cl_2CS was determined from a combination of electron diffraction data and published microwave data by Nakata et al. [26]. Kwiatkowski and Leszczyski [2] used the ab initio HF and MP2 levels of theory with triple-ζ valence shell basis sets to report the molecular parameters and the vibrational IR spectra of XYCS (X = H, F, Cl and Br), for which the experimental understanding is still incomplete.

Selenocarbonyls have been useful building blocks in organic synthesis and as important intermediates in the synthesis of selenium-containing molecules [3]. Moreover, the interest in selenocarbonyls is also due to the ability of selenium to act as a redox catalyst in the biological function of selenoproteins [1]. Selenoformaldehyde has been subjected to both experimental and theoretical studies [1, 3, 20, 27–31]. The ionization potential of selenoformaldehyde obtained from electron energy loss spectrometry is reported to be 8.80 eV [32], while Rauk et al. [20] used post-Hartree–Fock computations with Huzinaga basis sets for selenium to calculate the adiabatic ionization potential (8.58 eV). Liao et al. [3] used the B3LYP/6-311G(*d*) method to determine the HOMO–LUMO gap of selenoformaldehyde as 3.23 eV. The molecular structure of selenocarbonyl fluoride, F_2CSe, studied using the electron diffraction is reported by Christnen et al. Liao et al. [3] used the B3LYP/6-311G(*d*) method, while Kwiatkowski and Leszczyski [2] used the HF and MP2 levels of theory with triple-ζ valence shell basis sets to report the molecular parameters and the vibrational IR spectra of XYCSe (X = H, F, Cl and Br). The energetics of the XYCZ (X,Y = H, F, Cl and Br; Z = O, S and Se) species remain elusive.

Telluroformaldehyde has not yet been structurally characterized [32] although it was first stabilized by coordination to transition-metal centers by Roper et al. in 1983 [33, 34]. The cycloaddition reactions of heavy ketones of tellurium forming novel compounds [35–37] and the discovery of synthetic organotellurium compounds showing great antioxidant properties [38] are catalyzing the study of tellurium compounds. The present research aims at providing accurate theoretical values for the molecular parameters (bond lengths and bond angles), singlet–triplet splittings, ionization potentials (IP_{ad} and $IP_{ad(ZPVE)}$), electron affinities (EA_{ad}, $EA_{ad(ZPVE)}$, VEA and VDE) of the X_2CTe and the XYCTe (X,Y = H, F, Cl, Br and CN) species.

2 Methodology

Density functional theory (DFT) and second-order Møller–Plesset perturbation theory (MP2) [39] computations were performed using the Gaussian 03 program [40] to fully optimize the species independently in the gas phase. The functionals used at the DFT level are B3LYP, BLYP and BHLYP [41–43]. All neutral ground state structures are characterized as minima on the corresponding potential energy surface by performing vibrational frequency analyses. In all the cases, an extended integration grid (199,974) is used, with very tight convergence criteria applied to these computations.

The double-ζ basis sets with polarization and diffuse functions, denoted as DZP++, are used for all atoms except for tellurium and iodine, where the LANL2DZdp ECP [44–46] and 6-311G(*d*,*p*) [47] basis sets are used. The double-ζ basis sets are constructed by augmenting the Huzinaga–Dunning–Hay [48–50] sets of contracted Gaussian functions with one set of *p* polarization functions for each H atom and one set of *d* polarization functions for each heavy atom, respectively ($\alpha_p(H) = 0.75$, $\alpha_d(C) = 0.75$, $\alpha_d(F) = 1.0$). Basis functions for chlorine were obtained from the Ahlrichs standard double-ζ sp set [51] with one set of *d*-like polarization functions ($\alpha_d(Cl) = 0.75$). For bromine and nitrogen, the Ahlrichs standard double-ζ spd set was appended with a set *d* polarization functions, $\alpha = 0.389$ and $\alpha = 0.800$, respectively. The double-ζ basis sets are further augmented

with diffuse functions, where each atom received one additional *s*-type and one additional set of *p*-type functions. Each H atom basis set is appended with one diffuse *s* function. The diffuse functions are determined in an even-tempered fashion following the prescription of Lee [52],

$$\alpha_{\text{diffuse}} = \frac{1}{2}\left(\frac{\alpha_1}{\alpha_2} + \frac{\alpha_2}{\alpha_3}\right)\alpha_1$$

where α_1, α_2 and α_3 are the three smallest Gaussian orbital exponents of the *s*- or *p*-type for a given atom ($\alpha_1 < \alpha_2 < \alpha_3$). Thus, $\alpha_s(H) = 0.04415, \alpha_s(C) = 0.43021, \alpha_p(C) = 0.36290$, $\alpha_s(F) = 0.10490, \alpha_p(F) = 0.0826, \alpha_s(Cl) = 0.50480, \alpha_p(Cl) = 0.50870$, $\alpha_s(Br) = 0.04691$, $\alpha_p(Br) = 0.04653$, $\alpha_s(N) = 0.06029$ and $\alpha_p(N) = 0.05148$.

The adiabatic ionization potentials are determined by:

$$\text{IP}_{\text{ad}} = E(\text{optimized mono-cation}) - E(\text{optimized neutral})$$

The neutral–anion energy differences are evaluated by the following energy differences. The adiabatic electron affinity is determined by:

i. EA_{ad} = E(optimized neutral) − E(optimized anion);

vertical electron affinity by:

ii. EA_{vert} = E(optimized neutral) − E(anion at optimized neutral geometry);

and the vertical detachment energy of the anion:

iii. VDE = E(neutral at optimized anion geometry) − E(optimized anion).

Additionally, zero-point vibrational energies (ZPVE) are evaluated at each level. The corrected ionization potential $\text{IP}_{\text{ad(ZPVE)}}$ and the corrected adiabatic electron affinities $\text{EA}_{\text{ad(ZPVE)}}$ are reported as follows:

I. $$\text{IP}_{\text{ad(ZPVE)}} = E(\text{optimized cation} + \text{ZPVE}_{\text{cation}}) - E(\text{optimized neutral} + \text{ZPVE}_{\text{neutral}})$$

II. $$\text{EA}_{\text{ad(ZPVE)}} = E(\text{optimized neutral} + \text{ZPVE}_{\text{neutral}}) - E(\text{optimized anion} + \text{ZPVE}_{\text{anion}})$$

Each singlet–triplet splitting is predicted as the energy difference between the neutral ground state and the lowest lying triplet state.

3 Results

This section comprises the results obtained from the computations for the X_2CTe and XYCTe (X,Y = H, F, Cl, Br and CN) systems. All these molecules have been optimized as neutral ground state structures and confirmed to have no imaginary vibrational frequencies.

3.1 H_2CTe, H_2CTe^+ and H_2CTe^-

The equilibrium geometries of the $^1A'$ state of H_2CTe, the $^3A''$ state of H_2CTe, the $^2B''$ state of the H_2CTe^+ cation and the $^2B'$ state of the H_2CTe^- anion are presented in Fig. 1. From the singlet to the triplet state, there is an increase in the C=Te bond length of 0.084 Å (MP2), 0.080 Å (B3LYP), 0.079 Å (BLYP) and 0.096 Å (BHLYP), while there is a decrease in the H–C–Te bond angle of 1.7° (MP2 and B3LYP) and 1.8° (BLYP and BHLYP). The C=Te bond of the $^2B'$ state of the H_2CTe^- anion is thus lengthened by 0.095, 0.109, 0.104 and 0.119 Å compared to the $^1A'$ state of telluroformaldehyde. The theoretical IP_{ad}, $\text{IP}_{\text{ad(ZPVE)}}$, EA_{ad}, $\text{EA}_{\text{ad(ZPVE)}}$, VEA, VDE and singlet-triplet splitting are summarized in Tables 1, 2, 3,4 and 5. The computed IP_{ad} and $\text{IP}_{\text{ad(ZPVE)}}$ values range from 7.28–8.28 eV to 7.27–8.27 eV, respectively, with MP2 and B3LYP as the lower and upper limits. The $\text{EA}_{\text{ad(ZPVE)}}$ values range from 0.70 to 1.54 eV in the order MP2 < BLYP < B3LYP < BHLYP. The EA_{vert} values range from 0.93 (BLYP) to 1.93 eV (MP2), and the VDE values range from 1.14 (BLYP) to 1.44 eV (BHLYP). The singlet–triplet splitting for H_2CTe ranges from 0.53 (MP2) to 1.03 eV (BLYP).

3.2 F_2CTe, F_2CTe^+ and F_2CTe^-

The equilibrium geometries of the $^1A'$ state of F_2CTe, $^3A''$ state of F_2CTe, $^2B''$ state of the F_2CTe^+ cation and $^2B'$ state of the F_2CTe^- anion are presented in Fig. 2. Structural changes between the $^1A'$ state of F_2CTe and its corresponding triplet include an increase of 0.191 Å (MP2) in the C=Te bond length, accompanying a decrease in the F–C–Te bond angle of 11.7° (MP2). From the $^1A'$ state of F_2CTe to the $^2B'$ state of the F_2CTe^- anion, the F–C–Te bond angle increases by 2.2° (BHLYP), while the F–C–F bond angle decreases by 4.5° (BHLYP). The $\text{IP}_{\text{ad(ZPVE)}}$ is predicted to be 7.72 eV (MP2) < 8.70 eV (BHLYP) < 8.71 eV (BLYP) < 8.89 eV (B3LYP). The $\text{EA}_{\text{ad(ZPVE)}}$ values range from 1.29 (B3LYP) to 1.84 eV (BHLYP), while the EA_{vert} predictions are 0.75 eV (BLYP) < 1.01 eV (B3LYP) < 1.06 eV (BHLYP) < 2.03 eV (MP2). The VDE values range from 1.46 to 2.14 eV with B3LYP and BLYP as the lower and upper bounds. The theoretical singlet–triplet gaps are 0.85 eV (MP2) < 1.10 eV (BHLYP) < 1.47 eV (BLYP) < 1.85 eV (B3LYP).

3.3 Cl_2CTe, Cl_2CTe^+ and Cl_2CTe^-

Figure 3 presents the equilibrium geometries of the $^1A'$ state of Cl_2CTe, $^3A''$ state of Cl_2CTe, $^2B''$ state of the Cl_2CTe^+ cation and $^2B'$ state of the Cl_2CTe^- anion. The $^1A'$ state of Cl_2CTe has a predicted C=Te bond length ranging from 1.955 to 1.984 Å in the order of

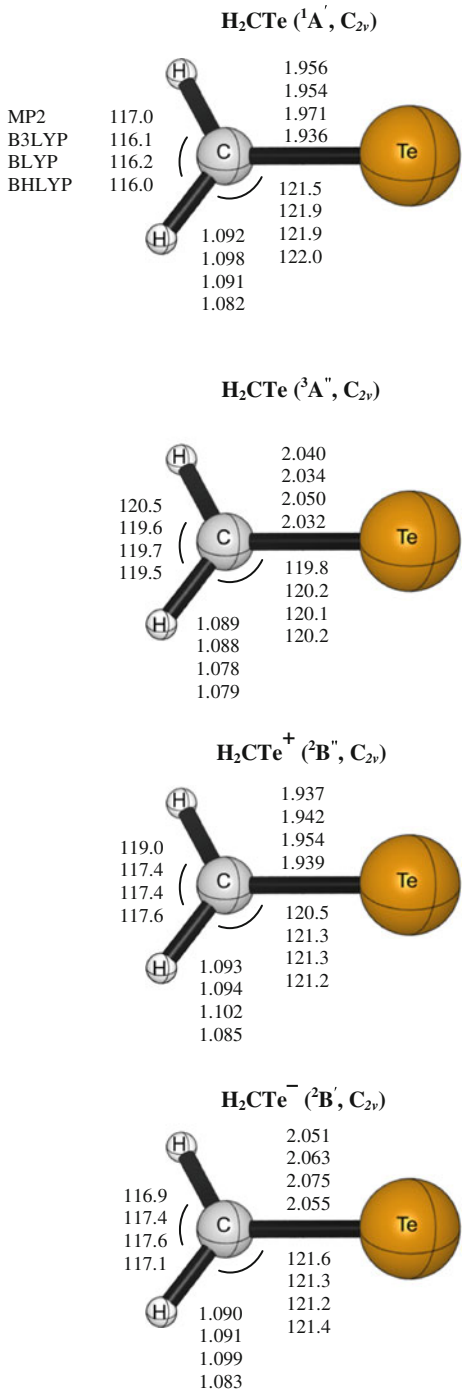

Fig. 1 Equilibrium geometries for the $^1A'$ state of H_2CTe, $^3A''$ state of H_2CTe, $^2B''$ state of the H_2CTe^+ cation and $^2B'$ state of the H_2CTe^- anion

BHLYP < B3LYP < MP2 < BLYP. The Cl–C–Te bond angle predictions are 124.0° (MP2 and BHLYP) ≈ 124.1° (B3LYP) < 124.3° (BLYP). The C–Cl bond lengths range from 1.717 (BHLYP) to 1.761 Å (BLYP). The $IP_{ad(ZPVE)}$ values range from 7.37 (MP2) to 8.38 eV (B3LYP). The Cl_2CTe molecule binds an electron with an $EA_{ad(ZPVE)}$ of 2.10 eV (BHLYP), VEA of 3.32 eV (MP2) and a VDE of 2.45 eV (MP2). The chlorinated singlet–triplet splitting is lower by 0.49 eV (B3LYP) than that of F_2CTe.

3.4 Br_2CTe, Br_2CTe^+ and Br_2CTe^-

The equilibrium geometries of the $^1A'$ state of Br_2CTe, $^3A''$ state of Br_2CTe, $^2B''$ state of the Br_2CTe^+ cation and $^2B'$ state of the Br_2CTe^- anion are presented in Fig. 4 (in the Supporting Information). From singlet to triplet state, there is an increase of 0.119 Å (B3LYP) in the C=Te bond length, 5.0° (BHLYP) in the Br–C–Br bond angle and a decrease of 7.1° in the Br–C–Te bond angle. The $IP_{ad(ZPVE)}$ values range from 7.12 (MP2) to 8.19 eV (B3LYP). The difference in electron affinity for Br_2CTe versus H_2CTe is 0.70 eV for the $EA_{ad(ZPVE)}$, 0.68 eV for the VEA and 1.11 eV for the VDE (B3LYP). The singlet–triplet gap is 0.16 eV (MP2) < 0.69 eV (BHLYP) < 1.02 eV (BLYP) < 1.07 eV (B3LYP).

3.5 I_2CTe, I_2CTe^+ and I_2CTe^-

Figure 5 (in the Supporting Information) presents the equilibrium geometries of $^1A'$ state of I_2CTe, $^3A''$ state of I_2CTe, $^2B''$ state of the I_2CTe^+ cation and $^2B'$ state of the I_2CTe^- anion. The $^1A'$ state of I_2CTe has predicted C–I bond length in the range 2.111–2.168 Å, while I–C–Te bond angle is in the range 123.2–123.8°, with BHLYP and BLYP as the lower and upper signposts. The addition of an extra electron to the neutral $^1A'$ state of I_2CTe molecule causes an increase in the C=Te and C–I bond distances by 0.085 Å (BHLYP) and 0.127 Å (B3LYP). The $IP_{ad(ZPVE)}$ values range from 6.31 (MP2) to 7.89 eV (B3LYP). The difference in electron affinity for I_2CTe versus H_2CTe is 1.34 eV (MP2) for the $EA_{ad(ZPVE)}$, 0.91 eV (BHLYP) for the VEA and 1.26 eV (MP2) for the VDE. The singlet–triplet gap is 0.08 eV (MP2) < 0.58 eV (BHLYP) < 0.87 eV (B3LYP) < 0.98 eV (BLYP).

3.6 $(NC)_2CTe$, $(NC)_2CTe^+$ and $(NC)_2CTe^-$

Turning to the di-cyano systems, Fig. 6 presents the equilibrium geometries of the $^1A'$ state of $(NC)_2CTe$, $^3A''$ state of $(NC)_2CTe$, $^2B''$ state of the $(NC)_2CTe^+$ cation and $^2B'$ state of the $(NC)_2CTe^-$ anion. For the neutral $^1A'$ state of $(NC)_2CTe$, the C=Te bond length ranges from 1.960 (BHLYP) to 2.014 Å (BLYP) and the C–C–Te bond angle falls in the range 121.8–122.0° (BHLYP). The C=Te bond distances for the X_2CTe species (X = H, F, Cl, Br, I and CN) are predicted in the systematic order 1.956 Å (H) < 1.961 Å (F) < 1.972 Å (Cl) < 1.974 Å (Br) < 1.978 Å (I) < 2.001 Å (CN), while the X–C–Te bond angle falls in the order 121.5° (H) < 122.0° (CN) < 123.4°

Table 1 Ionization potential (IP_{ad}) of X_2CTe and XYCTe (X,Y = H, F, Cl, Br, I and CN), in eV, where $IP_{ad(ZPVE)}$ is the adiabatic ionization potential corrected for zero-point vibrational energy contributions (in parentheses)

	MP2	B3LYP	BLYP	BH and HLYP
H_2CTe	7.28 (7.27)	8.28 (8.27)	8.11 (8.10)	8.27 (8.25)
F_2CTe	7.68 (7.72)	8.88 (8.89)	8.71 (8.72)	8.70 (8.71)
Cl_2CTe	7.38 (7.37)	8.37 (8.38)	8.16 (8.16)	8.24 (8.25)
Br_2CTe	7.10 (7.12)	8.18 (8.19)	7.96 (7.97)	8.07 (8.08)
I_2CTe	6.31 (6.31)	7.89 (7.89)	7.63 (7.63)	7.81 (7.81)
$(NC)_2CTe$	8.26 (8.46)	9.30 (9.26)	12.08 (12.07)	9.15 (9.12)
HFCTe	7.36 (7.38)	8.69 (8.70)	8.52 (8.53)	8.51 (8.51)
HClCTe	7.17 (7.18)	8.41 (8.41)	8.23 (8.23)	8.26 (8.26)
HBrCTe	7.08 (7.09)	8.31 (8.31)	8.12 (8.13)	8.16 (8.16)
HICTe	6.80 (7.00)	8.13 (8.13)	7.93 (7.93)	8.00 (8.00)
H(NC)CTe	7.78 (7.88)	8.85 (8.84)	8.63 (10.52)	8.68 (8.65)
FClCTe	7.50 (7.63)	8.61 (8.63)	8.42 (8.43)	8.46 (8.47)
FBrCTe	7.44 (7.63)	8.51 (8.52)	8.31 (8.32)	8.38 (8.38)
FICTe	7.20 (7.22)	8.34 (8.35)	8.11 (8.12)	8.23 (8.24)
F(NC)CTe	8.00 (8.15)	9.16 (9.16)	8.95 (8.95)	9.02 (9.01)
ClBrCTe	7.20 (7.84)	8.27 (8.28)	8.06 (8.07)	8.16 (8.16)
ClICTe	7.07 (7.09)	8.11 (7.62)	6.17 (6.18)	8.02 (8.02)
Cl(NC)CTe	7.79 (7.92)	8.87 (8.87)	8.66 (8.65)	8.75 (8.74)
BrICTe	7.54 (7.55)	8.03 (7.59)	7.79 (7.79)	7.94 (7.79)
Br(NC)CTe	7.70 (7.83)	8.76 (8.76)	8.53 (8.53)	8.64 (8.63)

Table 2 X_2CTe and XYCTe (X,Y = H, F, Cl, Br, I and CN) electron affinities E_{ad} and zero-point-corrected $EA_{ad(ZPVE)}$ values (in parentheses) in eV

	MP2	B3LYP	BLYP	BH and HLYP
H_2CTe	1.12 (0.70)	1.26 (1.32)	1.03 (1.28)	1.27 (1.54)
F_2CTe	1.31 (1.38)	1.22 (1.29)	1.25 (1.44)	1.56 (1.84)
Cl_2CTe	1.95 (1.98)	1.85 (1.43)	1.59 (1.77)	1.94 (2.10)
Br_2CTe	2.02 (2.05)	1.99 (2.02)	1.77 (1.93)	2.39 (2.53)
I_2CTe	2.01 (2.04)	2.11 (2.14)	1.67 (1.81)	2.15 (2.28)
$(NC)_2CTe$	3.09 (2.89)	3.34 (3.34)	3.05 (3.07)	3.39 (3.43)
HFCTe	1.30 (1.34)	1.29 (1.34)	1.04 (1.24)	1.35 (1.57)
HClCTe	1.56 (1.60)	1.55 (1.59)	1.29 (1.48)	1.61 (1.84)
HBrCTe	1.64 (1.67)	1.64 (1.68)	1.39 (1.56)	1.70 (1.90)
HICTe	1.69 (1.72)	1.71 (1.75)	1.46 (1.62)	1.77 (1.96)
H(NC)CTe	2.40 (2.35)	2.41 (2.44)	2.16 (2.26)	2.43 (2.56)
FClCTe	1.78 (1.82)	1.67 (1.72)	1.44 (1.62)	1.76 (1.93)
FBrCTe	1.85 (1.88)	1.77 (1.81)	1.55 (1.73)	1.84 (2.00)
FICTe	1.87 (1.91)	1.85 (1.92)	1.65 (1.80)	1.90 (2.06)
F(NC)CTe	2.60 (2.56)	2.46 (2.49)	2.20 (2.32)	2.51 (2.66)
ClBrCTe	1.99 (2.02)	1.92 (1.95)	1.69 (1.85)	2.00 (2.15)
ClICTe	2.00 (2.03)	1.98 (2.04)	1.77 (1.92)	2.04 (2.19)
Cl(NC)CTe	2.73 (2.67)	2.63 (2.65)	2.36 (2.46)	2.69 (2.80)
BrICTe	2.02 (2.04)	2.04 (2.08)	1.85 (2.00)	2.10 (2.23)
Br(NC)CTe	2.76 (2.70)	2.67 (2.69)	2.40 (2.50)	2.73 (2.84)

(I) < 124.0° (Cl) ≈ 124.1° (Br) < 126.3° (F). The trend in $IP_{ad(ZPVE)}$ is 6.31 eV (I) < 7.12 eV (Br) < 7.27 eV (H) < 7.38 eV (Cl) < 7.72 eV (F) < 8.46 eV (CN). The $EA_{ad(ZPVE)}$ for the X_2CTe species (X = H, F, Cl, Br, I and CN) fall in the order 0.70 eV (H) < 1.38 eV (F) < 1.98 eV (Cl) < 2.04 eV (I) ≈ 2.05 eV (Br) < 2.98 eV (CN). The singlet–triplet splitting of $(NC)_2CTe$ ranges from 0.10 (MP2) to 0.55 eV (BLYP).

Table 3 X_2CTe and XYCTe (X,Y = H, F, Cl, Br, I and CN) vertical electron affinities (VEA) in eV (kcal mol^{-1} in parentheses)

	MP2	B3LYP	BLYP	BH and HLYP
H_2CTe	1.93 (44.51)	1.14 (26.29)	0.93 (21.38)	1.12 (25.85)
F_2CTe	2.03 (46.73)	1.01 (23.18)	0.75 (17.41)	1.06 (24.33)
Cl_2CTe	3.32 (76.54)	1.69 (39.05)	1.40 (32.27)	1.78 (41.16)
Br_2CTe	1.10 (25.41)	1.82 (41.93)	1.52 (35.09)	1.91 (44.02)
I_2CTe	1.39 (31.94)	1.93 (44.40)	1.61 (37.23)	2.03 (46.92)
$(NC)_2CTe$	1.49 (34.32)	3.26 (75.25)	2.99 (68.87)	3.30 (76.00)
HFCTe	1.57 (36.13)	1.08 (25.02)	0.85 (19.50)	1.11 (25.71)
HClCTe	2.28 (52.50)	1.41 (32.48)	1.15 (26.56)	1.45 (33.49)
HBrCTe	1.53 (35.25)	1.50 (34.63)	1.24 (28.65)	1.55 (35.67)
HICTe	1.62 (37.35)	1.58 (36.55)	1.31 (30.22)	1.63 (37.64)
H(NC)CTe	1.68 (38.82)	2.31 (53.36)	2.07 (47.82)	2.31 (53.22)
FClCTe	2.46 (56.78)	1.38 (31.91)	1.11 (25.53)	1.47 (33.83)
FBrCTe	1.86 (42.97)	1.46 (33.69)	1.18 (27.27)	1.55 (35.71)
FICTe	1.91 (44.05)	1.39 (31.95)	1.24 (28.52)	1.62 (37.37)
F(NC)CTe	2.62 (60.39)	2.31 (53.37)	2.07 (47.67)	2.33 (53.81)
ClBrCTe	1.98 (45.58)	1.75 (40.47)	1.46 (33.69)	1.85 (42.59)
ClICTe	2.66 (61.30)	1.81 (41.71)	1.51 (34.75)	1.90 (43.88)
Cl(NC)CTe	1.93 (44.51)	2.52 (58.19)	2.26 (52.04)	2.56 (58.99)
BrICTe	2.03 (46.73)	1.87 (43.14)	1.56 (36.08)	1.97 (45.32)
Br(NC)CTe	3.32 (76.54)	2.57 (59.30)	2.30 (53.13)	2.61 (60.24)

Table 4 X_2CTe and XYCTe (X,Y = H, F, Cl, Br, I and CN) vertical detachment energies (VDE) in eV (kcal mol^{-1} in parentheses)

	MP2	B3LYP	BLYP	BH and HLYP
H_2CTe	1.29 (29.79)	1.39 (31.99)	1.14 (26.21)	1.44 (33.20)
F_2CTe	1.76 (40.56)	1.46 (33.74)	2.14 (49.27)	1.85 (42.65)
Cl_2CTe	2.45 (56.49)	2.16 (49.86)	2.20 (50.84)	2.35 (54.11)
Br_2CTe	2.56 (58.95)	2.50 (57.77)	2.44 (56.25)	2.80 (64.47)
I_2CTe	2.55 (58.82)	2.62 (60.47)	1.74 (40.17)	2.48 (57.21)
$(NC)_2CTe$	3.59 (82.69)	3.41 (78.64)	3.11 (71.73)	3.48 (80.28)
HFCTe	1.97 (45.54)	1.73 (39.90)	1.51 (34.84)	1.83 (42.11)
HClCTe	1.90 (43.91)	1.86 (42.84)	1.68 (38.70)	1.90 (43.72)
HBrCTe	2.04 (47.09)	1.99 (45.97)	1.85 (42.55)	2.00 (46.17)
HICTe	2.07 (47.72)	2.08 (47.94)	1.94 (44.81)	2.06 (47.50)
H(NC)CTe	2.27 (52.36)	2.51 (57.91)	2.24 (51.67)	2.56 (59.13)
FClCTe	2.62 (60.44)	2.39 (55.13)	2.23 (51.39)	2.45 (56.57)
FBrCTe	2.70 (62.25)	2.51 (57.82)	2.39 (55.19)	2.52 (58.22)
FICTe	2.69 (61.95)	2.60 (59.85)	2.49 (57.32)	2.56 (59.01)
F(NC)CTe	2.61 (60.20)	2.61 (60.19)	2.33 (53.62)	2.70 (62.28)
ClBrCTe	2.52 (58.12)	2.42 (55.83)	2.34 (53.98)	2.40 (55.41)
ClICTe	2.50 (57.54)	2.49 (57.44)	2.44 (56.24)	2.35 (54.12)
Cl(NC)CTe	2.60 (59.96)	2.75 (63.32)	2.46 (56.83)	2.83 (65.26)
BrICTe	1.56 (35.96)	2.56 (59.11)	2.51 (57.79)	2.46 (56.80)
Br(NC)CTe	2.61 (60.16)	2.78 (64.08)	2.50 (57.59)	2.86 (65.96)

3.7 HFCTe, $HFCTe^+$ and $HFCTe^-$

The equilibrium geometries of the $^1A'$ state of HFCTe, $^3A''$ state of HFCTe, $^2B''$ state of the $HFCTe^+$ cation and $^2B'$ state of the $HFCTe^-$ anion are displayed in Fig. 7. The $^1A'$ HFCTe structure has predicted C=Te and C–F bond distances in the range 1.940–1.969 Å and 1.318–1.361 Å with BHLYP and BLYP as the lower and upper bounds. The H–C–Te and F–C–Te bond angles fall in the order 125.3° (BHLYP) < 125.8° (B3LYP) < 126.2° (MP2) < 126.3°

Table 5 X_2CTe and XYCTe (X,Y = H, F, Cl, Br, I and CN) singlet–triplet gaps in eV ($kcalmol^{-1}$ in parentheses)

	MP2	B3LYP	BLYP	BH and HLYP
H_2CTe	0.53 (12.17)	0.92 (21.13)	1.03 (23.73)	0.70 (16.06)
F_2CTe	0.85 (19.51)	1.85 (42.77)	1.47 (33.84)	1.10 (25.42)
Cl_2CTe	0.32 (7.31)	1.36 (31.27)	1.21 (27.91)	0.77 (17.79)
Br_2CTe	0.16 (3.58)	1.07 (24.61)	1.02 (23.45)	0.69 (15.90)
I_2CTe	0.08 (1.86)	0.87 (20.04)	0.98 (22.56)	0.58 (13.28)
$(NC)_2CTe$	0.10 (2.32)	0.43 (10.02)	0.55 (12.62)	0.21 (4.83)
HFCTe	0.26 (6.05)	1.33 (30.72)	1.47 (33.97)	1.06 (24.46)
HClCTe	0.23 (5.29)	1.12 (25.81)	1.27 (29.28)	0.84 (19.41)
HBrCTe	0.16 (3.78)	1.07 (24.70)	1.22 (28.15)	0.79 (18.30)
HICTe	0.04 (0.90)	1.00 (23.06)	1.15 (26.41)	0.73 (16.74)
H(NC)CTe	0.14 (3.23)	0.64 (14.81)	0.76 (17.50)	0.41 (9.51)
FClCTe	0.10 (2.24)	1.24 (28.69)	1.37 (31.55)	0.97 (22.26)
FBrCTe	0.06 (1.36)	1.20 (27.64)	1.31 (30.19)	0.93 (21.36)
FICTe	0.05 (1.18)	1.13 (26.07)	1.25 (28.74)	0.90 (20.78)
F(NC)CTe	0.19 (4.41)	0.95 (21.94)	1.09 (25.19)	0.68 (15.66)
ClBrCTe	0.43 (9.85)	1.02 (23.61)	1.16 (26.73)	0.73 (16.87)
ClICTe	0.24 (5.65)	0.97 (22.45)	1.09 (25.18)	0.69 (15.90)
Cl(NC)CTe	0.40 (9.30)	0.74 (17.16)	0.89 (20.48)	0.47 (10.88)
BrICTe	0.36 (8.29)	0.93 (21.41)	1.04 (24.09)	0.64 (14.86)
Br(NC)CTe	0.26 (5.97)	0.71 (16.34)	0.85 (19.69)	0.44 (10.06)

(BLYP) and 123.9° (MP2) < 124.2° (BLYP) ≈ 124.3° (B3LYP) < 124.5° (BHLYP), respectively. From singlet to triplet state, there is an increase of 0.147 Å (MP2) in the C=Te bond length and a decrease of 7.9° (BLYP) and 8.4° (MP2 and BHLYP) in the H–C–Te and F–C–Te bond angles, respectively. The $IP_{ad(ZPVE)}$ values range from 7.38 (MP2) to 8.70 eV (B3LYP). The HFCTe molecule binds an extra electron, with the $EA_{ad(ZPVE)}$ ranging from 1.24 (BLYP) to 1.57 eV (BLYP) and the VEA and VDE ranging from 1.15 (BLYP) to 2.28 eV (MP2) and 1.51 eV (BLYP) to 1.97 eV (MP2), respectively. The singlet–triplet gap is predicted in the order 0.26 eV (MP2) < 1.06 eV (BHLYP) < 1.33 eV (B3LYP) < 1.47 eV (BLYP).

3.8 HClCTe, $HClCTe^+$ and $HClCTe^-$

The equilibrium geometries of the $^1A'$ state of HClCTe, $^3A''$ state of HClCTe, $^2B''$ state of the $HClCTe^+$ cation and $^2B'$ state of the $HClCTe^-$ anion are presented in Fig. 8. The neutral ground state $^1A'$ HClCTe has the C=Te and C–Cl bond lengths in the range 1.943–1.974 Å and 1.712–1.757 Å with BHLYP and BLYP as the lower and upper boundaries. The H–C–Te and Cl–C–Te bond angles are in the range 121.9–122.8° and 126.8–127.4° with MP2 and BLYP as the lower and upper limits. The removal of an electron from the HClCTe molecule causes an increase in the C=Te bond length by 0.033 Å and the Cl–C–Te bond angle by 5.3°, while the H–C–Te bond angle decreases by 4.4° (BLYP). The $IP_{ad(ZPVE)}$ values range from 7.18 (MP2) to 8.41 eV (B3LYP). The electron affinities $EA_{ad(ZPVE)}$, VEA and VDE range from 1.48 (BLYP) to 1.84 eV (BHLYP), 1.15 eV (BLYP) to 2.28 eV (MP2) and 1.68 eV (BLYP) to 1.90 eV (MP2 and BHLYP), respectively. The singlet–triplet splitting falls in the order 0.23 eV (MP2) < 0.84 eV (BHLYP) < 1.12 eV (B3LYP) < 1.27 eV (BLYP).

3.9 HBrCTe, $HBrCTe^+$ and $HBrCTe^-$

The equilibrium geometries of the $^1A'$ state of HBrCTe, $^3A''$ state of HBrCTe, $^2B''$ state of the $HBrCTe^+$ cation, and $^2B'$ state of the $HBrCTe^-$ anion are presented in Fig. 9 (in the Supporting Information). The differences in the geometrical parameters between the neutral ground state and the triplet state show an increase in the C=Te bond length by 0.101 Å accompanied by a decrease in the H–C–Te bond angle of 3.8° (MP2). Between the ground state neutral and the anion, there is an increase of 0.102 Å (BHLYP) in the C=Te bond length, accompanying a slight decrease in the Br–C–Te bond angle of 4.9° (BLYP). For HBrCTe, the ZPVE-corrected adiabatic electron affinity ranges from 1.56 (BLYP) to 1.90 eV (BHLYP), while the VEA values fall in the range 1.24–1.55 eV in the order BLYP < B3LYP < MP2 < BHLYP, and the VDE ranges from 1.85 (BLYP) to 2.04 eV (MP2). The singlet–triplet gap falls in the range 0.16 eV (MP2)–1.22 eV (BLYP).

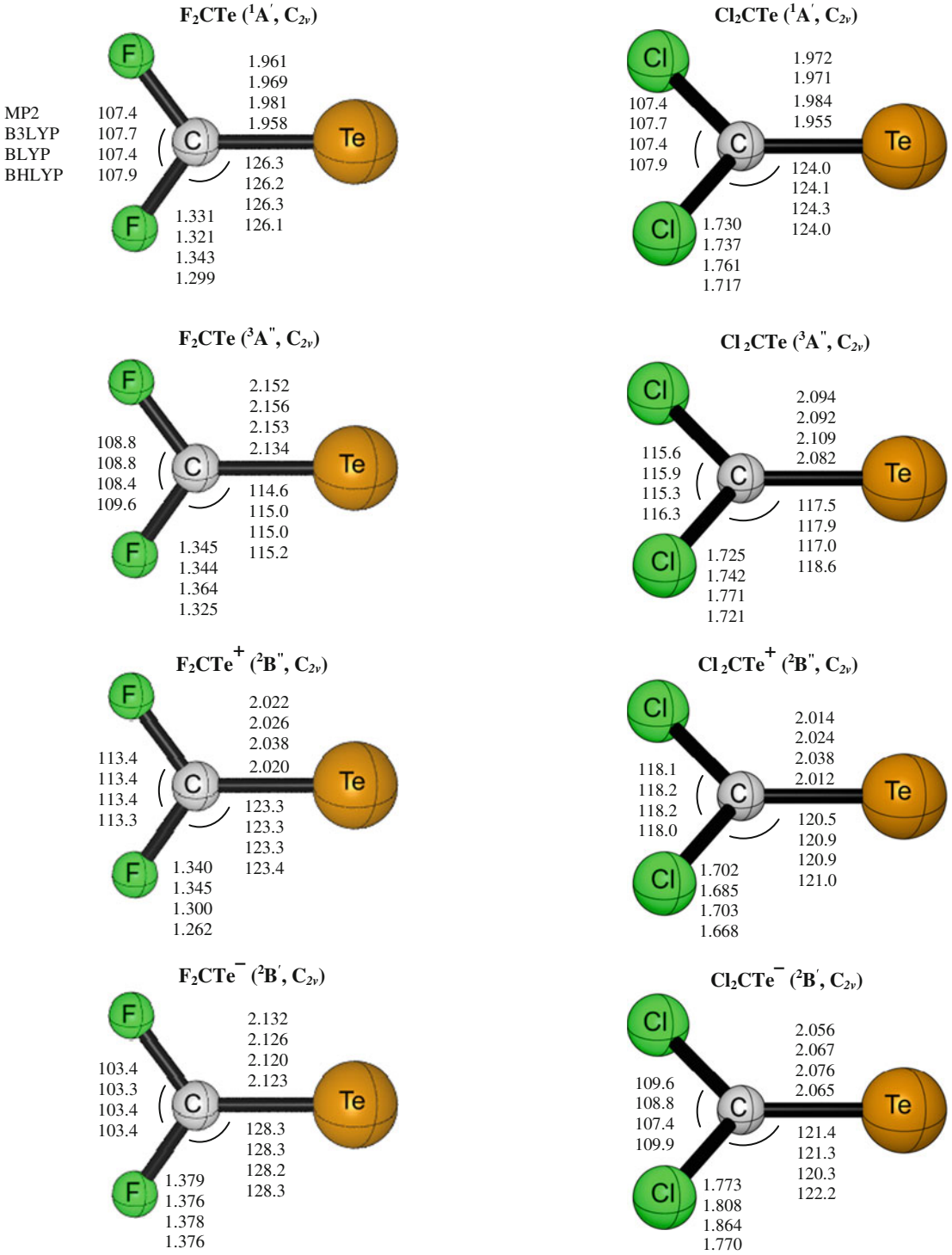

Fig. 2 Equilibrium geometries for the $^1A'$ state of F_2CTe, $^3A''$ state of F_2CTe, $^2B''$ state of the F_2CTe^+ cation and $^2B'$ state of the F_2CTe^- anion

Fig. 3 Equilibrium geometries for the $^1A'$ state of Cl_2CTe, $^3A''$ state of Cl_2CTe, $^2B''$ state of the Cl_2CTe^+ cation and $^2B'$ state of the Cl_2CTe^- anion

3.10 HICTe, $HICTe^+$ and $HICTe^-$

Figure 10 (in the Supporting Information) displays the equilibrium geometries of the $^1A'$ state of HICTe, $^3A''$ state of HICTe, $^2B''$ state of the $HICTe^+$ cation and $^2B'$ state of the $HICTe^-$ anion. Between the singlet ground state and lowest triplet state, there is a sizable increase in the C=Te bond length of 0.094 Å, while the I–C–Te bond angle is predicted to decrease by 12.7° (BLYP). The equilibrium geometry of the $HICTe^+$ ($^2B''$) cation reveals a decrease of

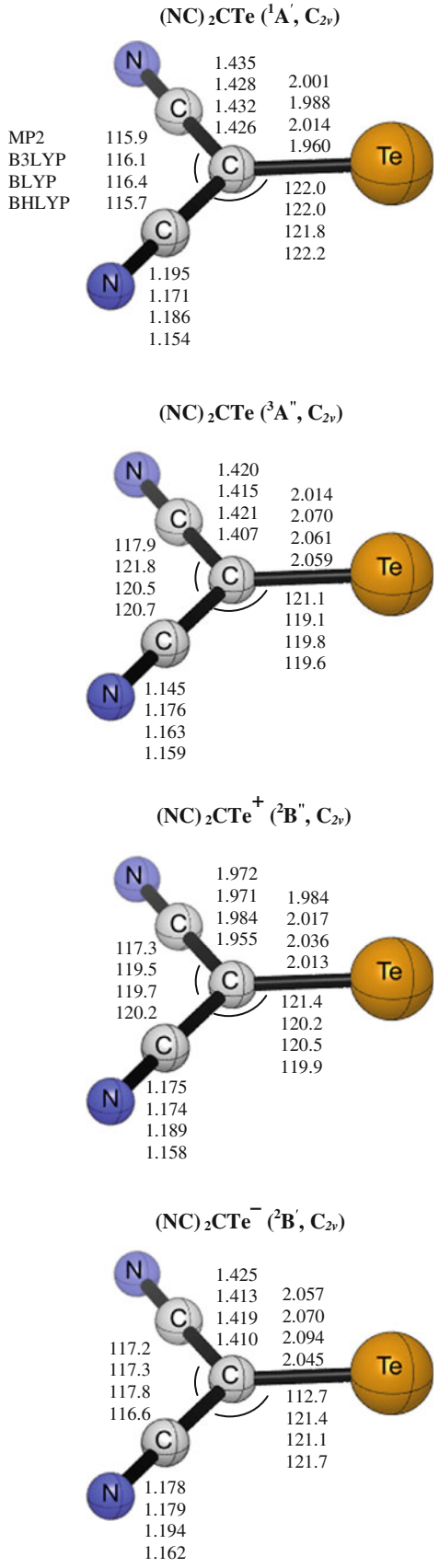

Fig. 6 Equilibrium geometries for the $^1A'$ state of $(NC)_2CTe$, $^3A''$ state of $(NC)_2CTe$, $^2B''$ state of the $(NC)_2CTe^+$ cation and $^2B'$ state of the $(NC)_2CTe^-$ anion

3.7° (B3LYP and BHLYP) in H–C–Te bond angle compared to the neutral ground state. A systematic increase is observed in the X–C–Te bond angle, in the range 123.9–128.3° (MP2), from HFCTe ($^1A'$) to HICTe ($^1A'$). It is noted that the $IP_{ad(ZPVE)}$ ranges from 7.00 to 8.13 eV in the order MP2 < BLYP < BHLYP < B3LYP. The predicted adiabatic ionization potential of the HXCTe molecules (X = F, Cl, Br, I) decreases systematically, 7.00 eV (I) < 7.09 eV (Br) < 7.18 eV (Cl) < 7.38 eV (F). The $EA_{ad(ZPVE)}$ increases in the order 1.34 eV (F) < 1.60 eV (Cl) < 1.67 eV (Br) < 1.72 eV (I) (MP2). For the singlet–triplet splitting both the DFT and MP2 computations reveal a systematic decrease.

3.11 H(NC)CTe, $H(NC)CTe^+$ and $H(NC)CTe^-$

The equilibrium geometries of the $^1A'$ state of H(NC)CTe, $^3A''$ state of H(NC)CTe, $^2B''$ state of the $H(NC)CTe^+$ cation and $^2B'$ state of the $H(NC)CTe^-$ anion are presented in Fig. 11. The geometries of the neutral ground state $^1A'$ H(NC)CTe show the C=Te bond length and the C–C–Te bond angle ranging from 1.946 (BHLYP) to 1.992 Å (BLYP) and 123.6° (MP2) to 124.5° (BLYP). The addition of an extra electron to $^1A'$ H(NC)CTe produces an increase of 0.099 Å in the C=Te bond length with a corresponding decrease in the C–C–Te bond angle of 1.0°. The predicted ZPVE-corrected ionization potential, the $EA_{ad(ZPVE)}$, VEA and VDE are in the range, 7.88 (MP2)–10.52 (BLYP) eV, 2.26 (BLYP)–2.56 (BHLYP) eV, 1.68 (MP2)–2.31 (B3LYP) eV and 2.24 (BLYP)–2.56 (BHLYP) eV, respectively. The singlet–triplet gap ranges from 0.14 (MP2) to 0.76 (BLYP) eV.

3.12 FClCTe, $FClCTe^+$ and $FClCTe^-$

The equilibrium geometries of the $^1A'$ state of FClCTe, $^3A''$ state of FClCTe, $^2B''$ state of the $FClCTe^+$ cation and $^2B'$ state of the $FClCTe^-$ anion are presented in Fig. 12. On comparing this F–C–Te bond angle with those of F_2CTe and HFCTe, the following trend is observed: 122.6° (FClCTe) < 123.9° (HFCTe) < 126.3° (F_2CTe) (MP2). The Cl–C–Te bond angle increases in the order 124.0° (Cl_2CTe) < 126.8° (HClCTe) < 128.2° (FClCTe). From the singlet to triplet state, an increase of 0.151 Å in the C=Te bond distance occurs, and the F–C–Cl bond angle is increased by 2.6° (B3LYP). The $IP_{ad(ZPVE)}$ values range from 7.63 to 8.63 eV. The electron affinities $EA_{ad(ZPVE)}$,

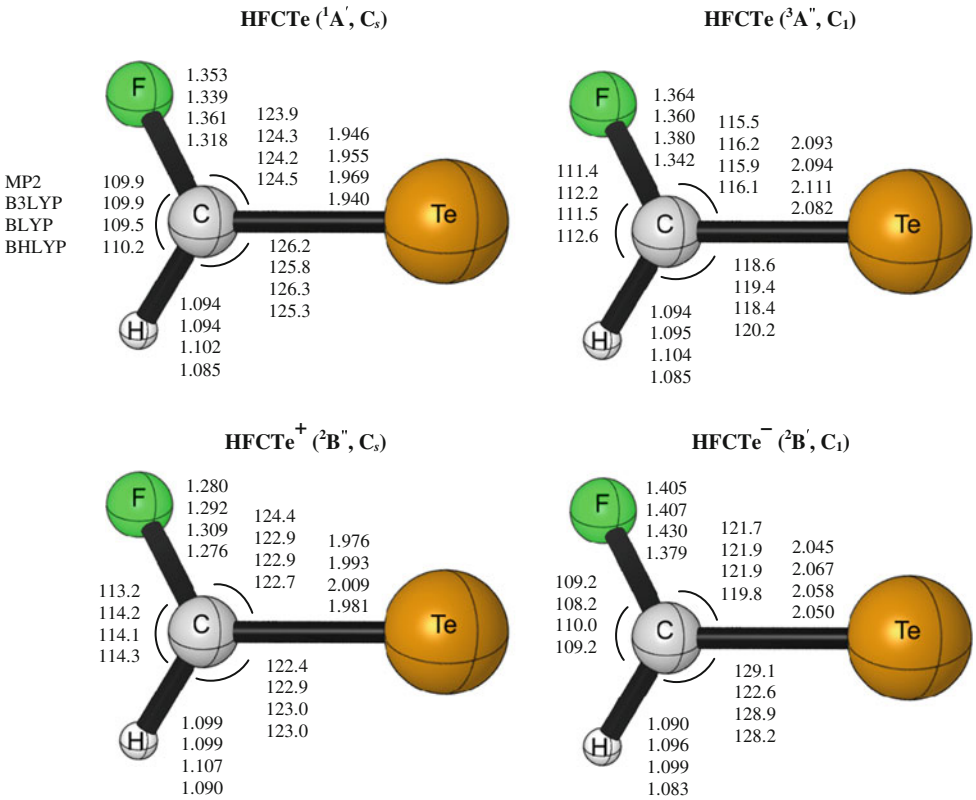

Fig. 7 Equilibrium geometries for the ^{1}A′ state of HFCTe, ^{3}A″ state of HFCTe, ^{2}B″ state of the HFCTe$^+$ cation and ^{2}B′ state of the HFCTe$^-$ anion

VEA and VDE range from 1.62 (BLYP) to 1.93 eV (BHLYP), 1.11 eV (BLYP) to 2.46 eV (MP2) and 2.23 eV (BLYP) to 2.62 eV (MP2), respectively. The singlet–triplet splitting ranges from 0.10 to 1.37 eV in the order MP2 < BHLYP < B3LYP < BLYP.

3.13 FBrCTe, FBrCTe$^+$ and FBrCTe$^-$

The optimized geometries of the ^{1}A′ state of FBrCTe, ^{3}A″ state of FBrCTe, ^{2}B″ state of the FBrCTe$^+$ cation and ^{2}B′ state of the FBrCTe$^-$ anion are displayed in Fig. 13 (in the Supporting Information). On comparing the geometrical parameters of ^{1}A′ FBrCTe with the neutral ground state of HBrCTe and Br_2CTe, it is noted that firstly, the C–Br bond length decreases systematically, 1.902 Å (Br_2CTe) > 1.892 Å (HBrCTe) > 1.890 Å (FBrCTe). Secondly, the Br–C–Te bond angle increases in the order 124.1° (Br_2CTe) < 127.1° (HBrCTe) < 128.1° (FBrCTe). Thirdly, the C=Te bond distance decreases with the trend (Br_2CTe) < (HBrCTe) ≈ (FBrCTe). From the neutral ground state to the triplet and FBrCTe$^+$ (^{2}B″), the F–C–Br bond angle decreases by 3.1° and 7.2° (BLYP), respectively. For FBrCTe, the ZPVE-corrected adiabatic ionization potential ranges from 7.63 to 8.52 eV. The $EA_{ad(ZPVE)}$ is predicted in the order 1.73 eV (BLYP) < 1.81 eV (B3LYP) < 1.88 eV (MP2) < 2.00 eV (BHLYP). The VEA and VDE range from 1.18–1.86 to 2.39–2.70 eV, respectively, with BLYP and MP2 acting as the lower and upper signposts. The singlet–triplet gap falls in the range 0.06 eV (MP2) to 1.31 eV (BLYP).

3.14 FICTe, FICTe$^+$ and FICTe$^-$

Figure 14 (in the Supporting Information) presents the optimized geometries of the ^{1}A′ state of FICTe, ^{3}A″ state of FICTe, ^{2}B″ state of the FICTe$^+$ cation and ^{2}B′ state of the FICTe$^-$ anion. On studying the ^{1}A′ I_2CTe, HICTe and FICTe molecules, a systematic gradual decrease is observed in the C=Te bond length, while the I–C–Te bond angle increases in the order 123.4° (I_2CTe) < 128.3° (HICTe) < 128.8° (FICTe). From the singlet to triplet state, the C=Te and the C–I bond distances are lengthened by 0.140 Å and 0.062 Å, respectively, reflecting increased bonding character. The loss of an electron from FICTe causes an increase in the C=Te bond length and F–C–I bond angle by 0.067 Å and 7.4° (MP2), respectively. The $IP_{ad(ZPVE)}$ values range from 7.20 to 8.34 eV. The $EA_{ad(ZPVE)}$ is predicted to be in the order 1.80 eV (BLYP) < 1.91 eV (MP2) < 1.92 eV (B3LYP) < 2.06 eV (BHLYP), while the VEA and VDE lie in the range 1.24–1.91 eV and 2.49–2.69 eV. The predicted $IP_{ad(ZPVE)}$ of the FXCTe species (X = Cl, Br, I) decreases gradually 8.63 eV (FClCTe) > 8.52 eV (FBrCTe) > 8.35 eV (FICTe), while the $EA_{ad(ZPVE)}$ increases in the order

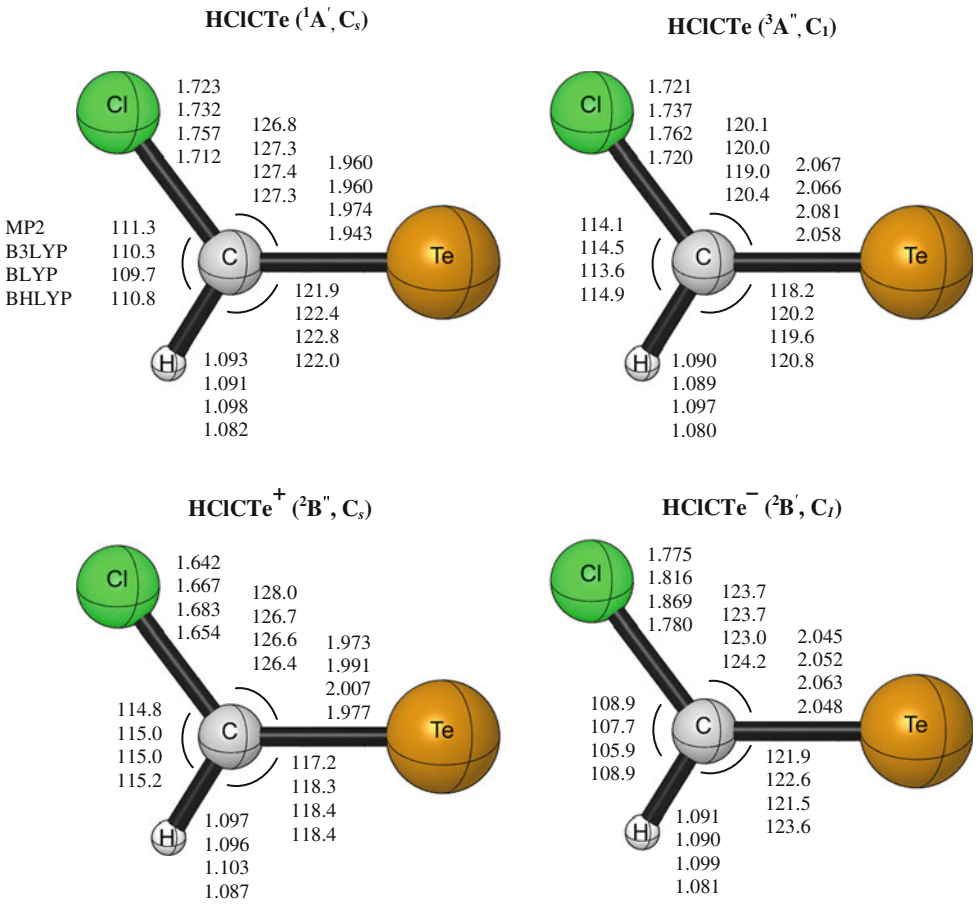

Fig. 8 Equilibrium geometries for the $^1A'$ state of HClCTe, $^3A''$ state of HClCTe, $^2B''$ state of the $HClCTe^+$ cation and $^2B'$ state of the $HClCTe^-$ anion

1.72 eV (FClCTe) < 1.81 eV (FBrCTe) < 1.92 eV (FICTe). The singlet–triplet gap of FICTe ranges from 0.05 to 1.25 eV with MP2 and BLYP as the lower and upper limits.

3.15 F(NC)CTe, F(NC)CTe$^+$ and F(NC)CTe$^-$

The equilibrium geometries of the $^1A'$ state of F(NC)CTe, $^3A''$ state of F(NC)CTe, $^2B''$ state of the F(NC)CTe$^+$ cation and $^2B'$ state of the F(NC)CTe$^-$ anion are displayed in Fig. 15. A systematic decrease in the C=Te bond length is observed in the FXCTe species (X = Cl, Br, I, CN). The B3LYP functional predicts the trend in C=Te bond distances to be 1.970 Å (FClCTe) > 1.968 Å (FBrCTe and FICTe) > 1.963 Å (F(NC)CTe). The F–C–Te and X–C–Te bond angles change in a fairly narrow range, 122.4° (FICTe) < 122.9° (F(NC)CTe) < 123.0° (FClCTe) ≈ 123.1° (FBrCTe) and 124.8° (F(NC)CTe) < 128.1° (FBrCTe) ≈ 128.2° (FClCTe) < 128.4° (FICTe), respectively. The $IP_{ad(ZPVE)}$ values range from 8.15 to 9.16 eV, while the $EA_{ad(ZPVE)}$ ranges from 2.32 to 2.66 eV. The VEA and the VDE values fall in the range 2.07–2.62 eV and 2.33–2.61 eV. The singlet–triplet gap falls in the range 0.19 eV (MP2) to 1.09 eV (BLYP).

3.16 ClBrCTe, ClBrCTe$^+$ and ClBrCTe$^-$

The optimized geometries of the $^1A'$ state of ClBrCTe, $^3A''$ state of ClBrCTe, $^2B''$ state of the ClBrCTe$^+$ cation and $^2B'$ state of the ClBrCTe$^-$ anion are presented in Fig. 16 (in the Supporting Information). The predicted C=Te bond length of the neutral ground state ClBrCTe is in the range 1.957–1.987 Å with BHLYP and BLYP as the bookends. The Br–C–Te bond angle is noted to be 3.7° less than that of FBrCTe molecule, while the C–Br bond length is 0.016 Å longer (MP2). A similar trend is observed while comparing the C–Cl bond length and Cl–C–Te bond angle of ClBrCTe with FClCTe. From singlet to triplet state, the C=Te bond distance and the Br–C–Cl bond angle increase by 0.120 Å and 4.6° (BHLYP), respectively. The $IP_{ad(ZPVE)}$ values range from 7.84 to 8.28 eV. The BrClCTe molecule binds an electron with the $EA_{ad(ZPVE)}$, 1.85–2.15 eV. The VEA and the VDE values are in the range 1.46–1.98 eV and 2.34–2.52 eV, respectively. The singlet–triplet gap

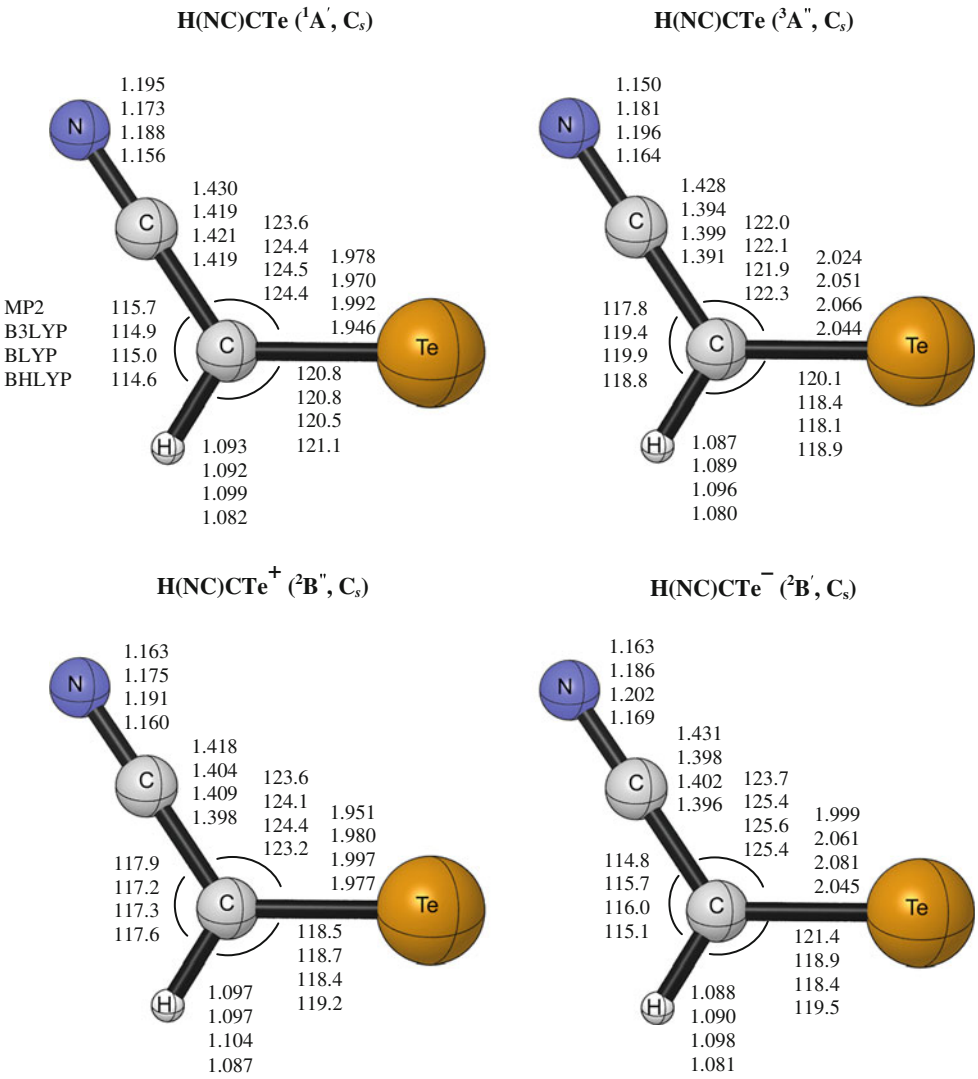

Fig. 11 Equilibrium geometries for the ^{1}A′ state of H(NC)CTe, ^{3}A″ state of the H(NC)CTe, ^{2}B″ state of the H(NC)CTe$^+$ cation and ^{2}B′ state of the H(NC)CTe$^-$ anion

falls in the range 0.43–1.16 eV in the order MP2 < BHLYP < B3LYP < BLYP.

3.17 ClICTe, ClICTe$^+$ and ClICTe$^-$

The equilibrium geometries of the ^{1}A′ state of ClICTe, ^{3}A″ state of ClICTe, ^{2}B″ state of the ClICTe$^+$ cation and ^{2}B′ state of the ClICTe$^-$ anion are presented in Fig. 17 (in the Supporting Information). The geometry of the neutral ground state ClICTe shows the C=Te, C–Cl and C–I bond distances ranging from 1.945 to 1.987 Å, 1.719–1.760 Å and 2.110–2.169 Å, respectively. The Cl–C–I, Cl–C–Te and I–C–Te bond angles fall in the ranges 111.6–112.6°, 123.1–123.7° and 124.1–124.7°, respectively. The loss of an electron from ^{1}A′ ClICTe leads to an increase of 0.045 Å and 6.5° in the C=Te bond length and the Cl–C–I bond angle. The ZPVE adiabatic ionization potential of ClICTe is decreased by 1.89 eV, while the $EA_{ad(ZPVE)}$, VEA and VDE are increased by 0.07 eV, 0.05 eV and 0.10 eV, respectively, compared to that for ClBrCTe with the BLYP functional. The VEA and the VDE of ClICTe fall in the ranges 1.51–2.66 eV and 2.44–2.50 eV, respectively. The singlet–triplet gap of ClICTe is 0.07 eV lower than that of ClBrCTe (BLYP).

3.18 Cl(NC)CTe, Cl(NC)CTe$^+$ and Cl(NC)CTe$^-$

Figure 18 presents the equilibrium geometries of the ^{1}A′ state of Cl(NC)CTe, ^{3}A″ state of Cl(NC)CTe, ^{2}B″ state of the Cl(NC)CTe$^+$ cation and ^{2}B′ state of the Cl(NC)CTe$^-$ anion. The comparison of the geometrical parameters of the neutral ground state of ClXCTe species (X = Br, I, CN) reveals that the C–Cl bond length and the Cl–C–X and Cl–C–Te bond angles increase systematically, 1.735 Å (ClBrCTe) < 1.738 Å (ClICTe) < 1.743 Å (Cl(NC)CTe), 111.7° (ClBrCTe) to 112.7° (Cl(NC)CTe) and 124.0–125.4°, respectively, with the B3LYP functional. The C=Te bond distance changes very little, 1.973 Å

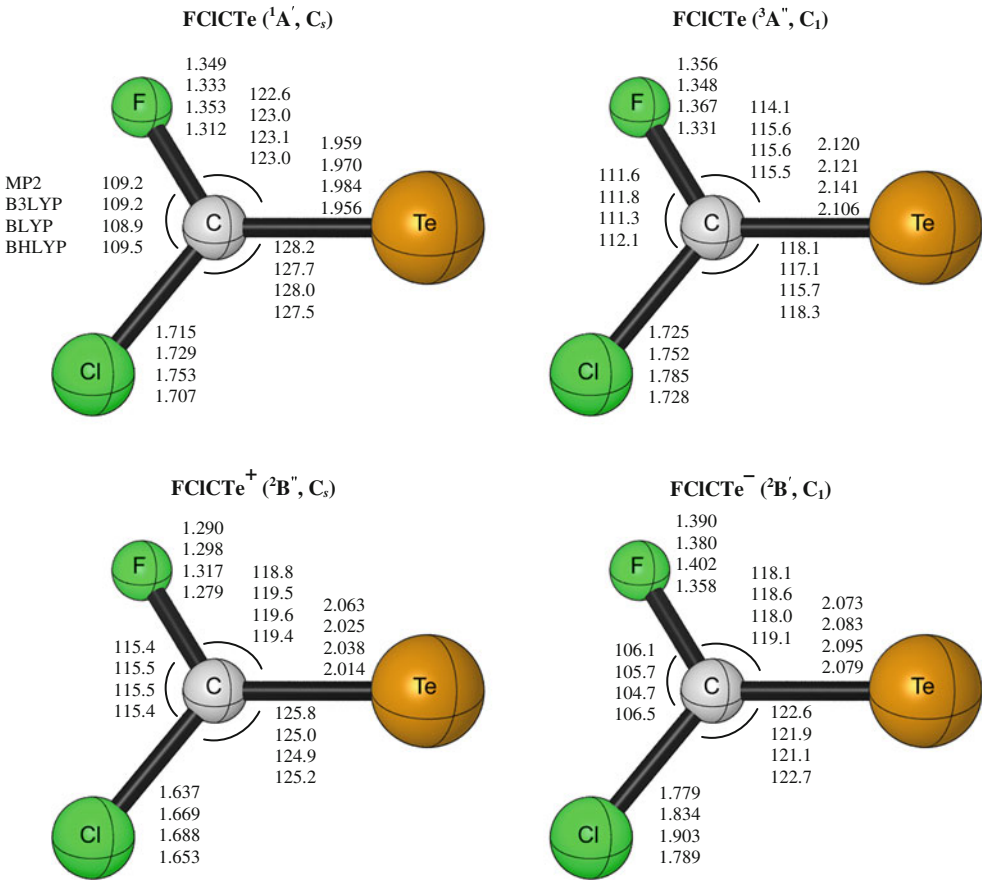

Fig. 12 Equilibrium geometries for the ^{1}A′ state of FClCTe, ^{3}A″ state of FClCTe, ^{2}B″ state of the FClCTe$^+$ cation and ^{2}B′ state of the FClCTe$^-$ anion

(ClICTe) < 1.974 (Cl(NC)CTe) < 1.976 (ClBrCTe). From ^{1}A′ Cl(NC)CTe to ^{2}B′ Cl(NC)CTe$^-$, the C=Te and C–Cl bond lengths increase by 0.064 and 0.075 Å. The $IP_{ad(ZPVE)}$ is predicted to be 7.92 eV (MP2) < 8.65 eV (BLYP) < 8.74 eV (BHLYP) < 8.87 eV (B3LYP). The Cl(NC)CTe molecule binds an extra electron with the $EA_{ad(ZPVE)}$, 2.46–2.80 eV. The VEA and the VDE values are in the ranges 1.93–2.56 eV and 2.46–2.83 eV, respectively. The singlet–triplet splitting of Cl(NC)CTe falls in the range 0.40 (MP2)–0.89 (BLYP) eV.

3.19 BrICTe, BrICTe$^+$ and BrICTe$^-$

The equilibrium geometries of the ^{1}A′ state of BrICTe, ^{3}A″ state of BrICTe, ^{2}B″ state of the BrICTe$^+$ cation and ^{2}B′ state of the BrICTe$^-$ anion are presented in Fig. 19 (in the Supporting Information). The geometry of the neutral ground state BrICTe shows the C=Te, C–Br and C–I bond distances ranging from 1.955 to 1.984 Å, 1.886 to 1.937 Å and 2.108 to 2.164 Å, respectively. The Br–C–I, Br–C–Te and I–C–Te bond angles fall in narrow ranges 111.8–112.8°, 122.9–123.4° and 124.2–124.8°, respectively. The study of the XBrCTe species (X = H, F, Cl, Br, I) reveals that the $IP_{ad(ZPVE)}$ values are predicted to be 7.09 eV (HBrCTe) < 7.12 eV (Br_2CTe) < 7.55 eV (IBrCTe) < 7.63 eV (FBrCTe) < 7.84 eV (ClBrCTe), and the $EA_{ad(ZPVE)}$ varies as 1.67 eV (HBrCTe) < 1.88 eV (FBrCTe) < 2.02 eV (ClBrCTe) < 2.04 eV (IBrCTe) < 2.05 eV (Br_2CTe). The singlet–triplet gap falls in the order 0.43 eV (ClBrCTe) < 0.36 eV (IBrCTe) < 0.26 eV (HBrCTe) < 0.16 eV (Br_2CTe) < 0.06 eV (FBrCTe).

3.20 Br(NC)CTe, Br(NC)CTe$^+$ and Br(NC)CTe$^-$

Figure 20 (in the Supporting Information) presents the equilibrium geometries of the ^{1}A′ state of Br(NC)CTe, ^{3}A″ state of Br(NC)CTe, ^{2}B″ state of the Br(NC)CTe$^+$ cation and ^{2}B′ state of the Br(NC)CTe$^-$ anion. The substitution of the halogen, I, by the –CN group causes an increase in the C=Te bond length and the Br–C–Te bond angle by 0.009 Å and 2.2°, while the C–Br bond distance decreases by 0.007 Å. In most cases, the BHLYP functional predicts the shortest bond distances and lowest $EA_{ad(ZPVE)}$ values, while the MP2 method predicts the lowest values for the ionization potentials, the VEA, VDE and singlet–triplet splitting. The $IP_{ad(ZPVE)}$ values of Br(NC)CTe range from 7.83 to 8.76 eV. The Br(NC)CTe molecule binds an electron with the $EA_{ad(ZPVE)}$, 2.50–2.84 eV. The VEA and the

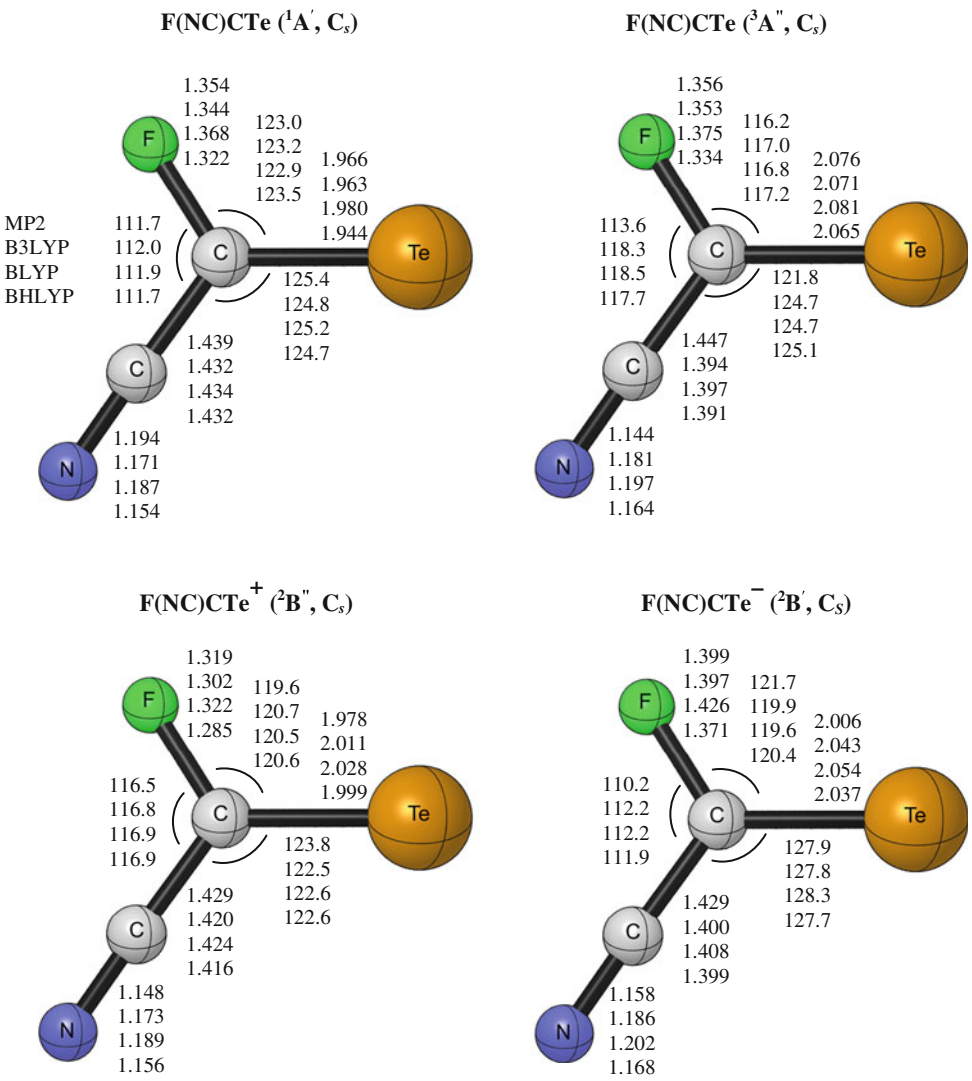

Fig. 15 Equilibrium geometries for the $^1A'$ state of F(NC)CTe, $^3A''$ state of F(NC)CTe, $^2B''$ state of the $F(NC)CTe^+$ cation and $^2B'$ state of the $F(NC)CTe^-$ anion

VDE values are in the range 2.30–3.32 eV and 2.50–2.86 eV, respectively. The singlet–triplet gap falls in the range 0.26–0.85 eV in the order MP2 < BHLYP < B3LYP < BLYP.

4 Discussion

This section comprises a systematic analysis and discussion of the structural parameters, ionization potentials, electron affinities and singlet–triplet gap of the X_2CTe and XYCTe (X,Y = H, F, Cl, Br, I and CN) systems.

4.1 Structural parameters

The predicted structural parameters of the X_2CTe molecules (X = H, F, Cl, Br, I and CN) show that the C=Te and C–X bond distances elongate in the order H < F < Cl < Br < I < CN. These expected trends are due to the change in atomic sizes and electronegativities (χ) of the halogen substituent. The electronegativity (χ) can be used as a noteworthy reactivity descriptor, qualitatively defined by Pauling [53]. The standard Pauling electronegativities lie in the order F(3.98) > Cl(3.16) > Br(2.96) > I(2.66) > C(2.55) > H(2.20). The X–C–Te bond angles of the X_2CTe species in their singlet ground states lie in the range 121.5–126.3° (MP2), with H_2CTe and F_2CTe acting as the bookends. The large electronegativity of fluorine decreases the electron density on carbon, and hence, the repulsion between the electron pairs is nullified, and the F–C–Te bond angle is increased. Comparison of these changes in the X–C–Te angles with the literature data of X_2CZ (Z = O, S and Se) is reported in Table 6; the agreement is acceptable.

For the geometrical parameters of the HXCTe species (X = F, Cl, Br, I, CN), nontrivial changes are observed. The MP2 method predicts that C=Te bond length increases in the order 1.946 Å (F) < 1.957 Å (Br) < 1.960 Å (Cl and

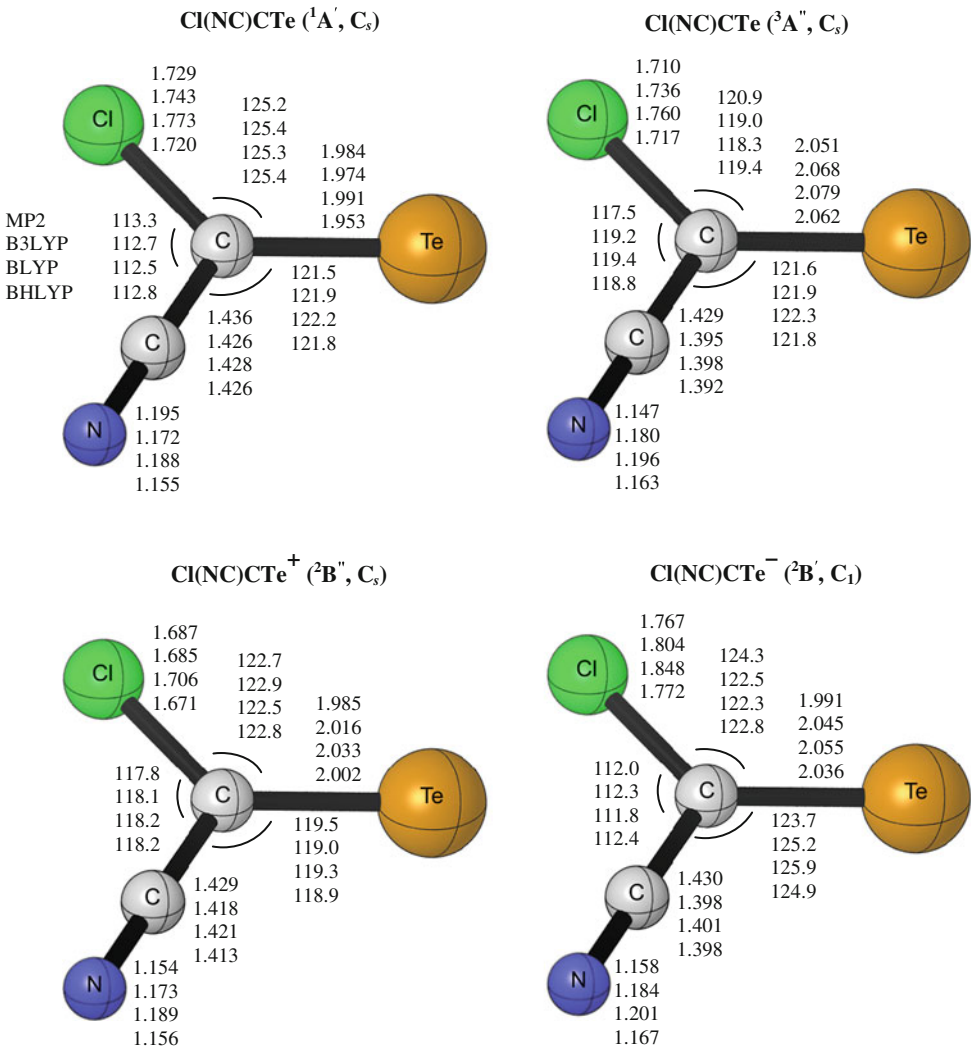

Fig. 18 Equilibrium geometries for the $^1A'$ state of Cl(NC)CTe, $^3A''$ state of Cl(NC)CTe, $^2B''$ state of the Cl(NC)CTe$^+$ cation and $^2B'$ state of the Cl(NC)CTe$^-$ anion

I) < 1.978 Å (CN), while the H–C–Te bond angle decreases in the order 126.2° (F) > 122.6° (Br) > 121.9° (Cl) > 121.4° (I) > 120.8° (CN). The change observed in the specified bond angle is consistent with the trend reported for HXCS species (X = F, Cl, Br) in Table 7. The structural parameters of the FXCTe species (X = Cl, Br, I, CN) reveal a systematic decrease in the C=Te bond length and uneven changes in the F–C–Te and X–C–Te bond angles.

On evaluating the structural parameters of the FXCTe and ClXCTe molecules with the literature results for FXCS and ClXCS (X = F, Cl and Br) reported in Table 7, a good correlation can be made. Analysis of the geometrical parameters of both ClXCTe and BrXCTe species indicates that the cyano-derivatives have the longest C=Te bond, a result rationalized by π electron acceptor ability of the ligand. Moreover, the cyano-derivatives are found to be the most electronegative species among the telluroformaldehyde compounds studied, when Mulliken's electronegativity is considered. The Mulliken's electronegativity, also termed as the absolute electronegativity, is calculated using the equation: $\chi_M = \frac{I+A}{2}$ [72]. Figure 21 illustrates the Mulliken's electronegativity of X_2CTe, HXCTe and FXCTe families.

Comparing the geometrical parameters of the lowest singlet and triplet states of the molecules, the most noticeable contrast is that the C=Te bond distance and the X–C–X bond angle are increased. In the singlet state, the HOMO is of a′ symmetry, corresponding to the lone pair of electrons lying in the molecular plane. Consequently, in the triplet state, an electron is moved to an orbital of a″ symmetry. As a result, of the valence shell electrons in the molecular plane, only one electron remains at the carbon center, leading to a large decrease in the repulsion, opening the bond angle in the triplet state. Another remarkable difference between the neutral ground and the lowest lying triplet state is that the X–C–Te bond angle is decreased in the triplet state. To study the influence of a given halide substituent on the bond length, it is useful to plot the values

Table 6 Structural parameters, ionization potentials and electron affinities (eV) of the X_2CZ analogues, where X = H, F, Cl and Br and Z = O, S and Se

Z	O	S	Se
H_2CZ	r(C–H) = 1.095 Å, r(C=O) = 1.179 Å, ∠(HCH) = 115.8° (calc) [1]	r(C–H) = 1.080 Å, r(C=S) = 1.596 Å, ∠(HCS) = 122.0° (calc) [2]	r(C–H)) = 1.077 Å, r(C=Se) = 1.734 Å, ∠(HCH) = 116.3° (calc) [1]
	r(C–H) = 1.106 Å, r(C=O) = 1.210 Å, ∠(HCH) = 115.7° (calc) [1]	r(C–H) = 1.090 Å, r(C=S) = 1.613 Å, ∠(HCS) = 121.9° (calc) [2]	r(C–H)) = 1.088 Å, r(C=Se) = 1.754 Å, ∠(HCH) = 117.1° (calc) [1]
	r(C–H) = 1.101 Å, r(C=O) = 1.203 Å, ∠(HCH) = 116.3° (expt) [27]	r(C–H) = 1.096 Å, r(C=S) = 1.614 Å, ∠(HCS) = 121.9° (expt) [63, 64]	r(C–H)) = 1.090 Å, r(C=Se) = 1.753 Å, ∠(HCH) = 117.9° (expt) [69]
	IP = 10.88 eV (expt) [9]	r(C–H) = 1.093 Å, r(C=S) = 1.611 Å, ∠(HCS) = 121.6° (expt) [63, 64]	IP = 8.80 eV (expt) [31]
	IP = 10.82 eV (calc) [10]	IP = 9.44 eV (expt) [19]	IP = 8.58 eV (calc) [20]
	EA = −0.65 eV (expt) [7]	IP = 9.08 eV (calc) [20]	
	EA = −0.96 eV (calc) [10]	EA = 0.47 eV (expt) [21]	
		EA = 0.38 eV (calc) [22]	
F_2CZ	r(C–F) = 1.285 Å, r(C=O) = 1.149 Å, ∠(FCF) = 108.3° (calc) [1]	r(C–F) = 1.281 Å, r(C=S) = 1.589 Å, ∠(FCS) = 126.0° (calc) [2]	r(C–F)) = 1.277 Å, r(C=Se) = 1.744 Å, ∠(FCF) = 108.3° (calc) [1]
	r(C–F) = 1.316 Å, r(C=O) = 1.175 Å, ∠(FCF) = 107.6° (calc) [1]	r(C–F) = 1.316 Å, r(C=S) = 1.593Å, ∠(FCS) = 126.4° (calc) [2]	r(C–F)) = 1.315 Å, r(C=Se) = 1.743 Å, ∠(FCF) = 107.8° (calc) [1]
	r(C–F) = 1.317 Å, r(C=O) = 1.170 Å, ∠(FCF) = 107.6° (expt) [57]	r(C–F) = 1.317 Å, r(C=S) = 1.589 Å, ∠(FCS) = 126.5° (expt) [63, 64]	r(C–F)) = 1.314 Å, r(C=Se) = 1.743 Å, ∠(FCF) = 107.5° (expt) [70]
	IP = 13.035 ± 0.030 eV (expt) [58]	IP = 10.30 eV (expt) [65]	IP = 9.40 eV (expt) [65]
		IP = 10.53 ± 0.10 (expt) [66]	
Cl_2CZ	r(C–Cl) = 1.740 Å, r(C=O) = 1.151 Å, ∠(ClCCl) = 113.0° (calc) [1]	r(C–Cl) = 1.725 Å, r(C=S) = 1.588 Å, ∠(ClCS) = 124.1° (calc) [2]	r(C–Cl) = 1.720 Å, r(C=Se) = 1.738 Å, ∠(ClCCl) = 112.3° (calc) [1]
	r(C–Cl) = 1.747 Å, r(C=O) = 1.183 Å, ∠(ClCCl) = 112.2° (calc) [1]	r(C–Cl) = 1.735 Å, r(C=S) = 1.604 Å, ∠(ClCS) = 124.2° (calc) [2]	r(C–Cl) = 1.729 Å, r(C=Se) = 1.756 Å, ∠(ClCCl) = 112.1° (calc) [1]
	r(C–Cl) = 1.738 Å, r(C=O) = 1.188 Å, ∠(ClCCl) = 112.2° (expt) [59]	r(C–Cl)=1.729 Å, r(C=S) = 1.602 Å, ∠(ClCS) = 124.4° (expt) [63, 64]	
	IP = 11.84 eV (expt) [60]	IP = 9.61 ± 0.02 eV (expt) [67]	
		IP = 9.68 eV (expt) [68]	
Br_2CZ	r(C–Br) = 1.920 Å, r(C=O) = 1.147 Å, ∠(BrCBr) = 113.5° (calc) [1]	r(C–Br) = 1.899 Å, r(C=S) = 1.583 Å, ∠(BrCS) = 123.9° (calc) [2]	r(C–Br) = 1.890 Å, r(C=Se) = 1.734 Å, ∠(BrCS) = 112.6° (calc) [1]
	r(C–Br) = 1.931 Å, r(C=O) = 1.178 Å, ∠(BrCBr) = 112.3° (calc) [1]	r(C–Br) = 1.912 Å, r(C=S) = 1.600 Å, ∠(BrCS) = 124.4° (calc) [2]	r(C–Br) = 1.903 Å, r(C=Se) = 1.753 Å, ∠(BrCS) = 112.0° (calc) [1]
	r(C–Br) = 1.917 Å, r(C=O) = 1.176 Å, ∠(BrCBr) = 112.4° (expt) [61]	r(C–Br) = 1.894 Å, r(C=S) = 1.597 Å, ∠(BrCS) = 124.2° (expt) [63, 64]	
	IP = 10.80 eV(expt) [62]		

of the C=Te bond distance for the X_2CTe and XYCTe species (X, Y = H, F, Cl, Br, I and CN) as a function of the Pauling electronegativity of the substituent X. Similarly, in keeping the r(C=Te) bond distance fixed, the trend in the C–X bond elongation can be analyzed. Figures 22 and 23 show the influence of the substituents on the C=Te and C–X bond distances for the X_2C=Te and HXC=Te species (X, Y = H, F, Cl, Br, I and CN). The substituents X and/or Y that get closer to the carbon atom due to the electronegativity difference, achieve a better screening of the bonding electrons. Comparison with experimental structural parameters is not possible, since no literature results are available for triplet states of the X_2CZ or XYCZ (X, Y = H, F, Cl, Br, I and CN and Z = O, S and Se) systems.

4.2 Ionization potentials

Table 1 reports the ionization potentials for the X_2CTe and XYCTe species (X,Y = H, F, Cl, Br, I and CN). The largest ionization potential appears in the case of the fluoro- and cyano-telluroformaldehyde derivatives. The ionization potential of molecules studied in this research fall in the order CN > F > Cl > Br > I, in agreement with the Pauling electronegativities of the halogens and the strong field ligand properties of CN and F. The presence of a strongly electron-withdrawing atom or a strong π acceptor ligand, being directly attached to the carbonyl carbon, reduces the population of the 2*s* and 2*p* orbitals of the carbon center. Thus, the carbonyl carbon becomes more electron deficient and the ability to remove an electron decreases.

Table 7 Structural parameters of the HXCZ analogues (X = F, Cl and Br and Z = S and Se)

Z	S	Se
HFCZ	r(C–H) = 1.078 Å, r(C=S) = 1.586 Å, r(C–F) = 1.302 Å, ∠(HCS) = 125.5°, ∠(FCS) = 124.1° (calc) [2] r(C–H) = 1.089 Å, r(C=S) = 1.596 Å, r(C–F) = 1.337 Å, ∠(HCS) = 126.3°, ∠(FCS) = 124.0° (calc) [2]	r(C–H) = 1.090 Å, r(C=Se) = 1.750 Å, r(C–F) = 1.330 Å, ∠(HCSe) = 125.8°, ∠(FCSe) = 124.3° (calc) [3]
HClCZ	r(C–H) = 1.076 Å, r(C=S) = 1.587 Å, r(C–Cl) = 1.727 Å, ∠(HCS) = 123.6°, ∠(ClCS) = 125.8° (calc) [2] r(C–H) = 1.088Å, r(C=S) = 1.603 Å, r(C–Cl) = 1.735 Å, ∠(HCS) = 123.8°, ∠(ClCS) = 125.8° (calc) [2]	r(C–H) = 1.090 Å, r(C=Se) = 1.750 Å, r(C–Cl) = 1.740 Å, ∠(HCSe) = 123.4°, ∠(ClCSe) = 126.4° (calc) [3]
HBrCZ	r(C–H) = 1.076 Å, r(C=S) = 1.584 Å, r(C–Br) = 1.898 Å, ∠(HCS) = 124.0°, ∠(BrCS) = 126.0° (calc) [2] r(C–H) = 1.088 Å, r(C=S) = 1.599 Å, r(C–Br) = 1.914 Å, ∠(HCS) = 124.8°, ∠(BrCS) = 125.9° (calc) [2]	r(C–H) = 1.090 Å, r(C=Se) = 1.750 Å, r(C–Br) = 1.910 Å, ∠(HCSe) = 123.5°, ∠(BrCSe) = 127.0° (calc) [3]
FClCZ	r(C–F) = 1.293 Å, r(C=S) = 1.586 Å, r(C–Cl) = 1.715 Å, ∠(FCS) = 123.8°, ∠(ClCS) = 126.8° (calc) [2] r(C–F) = 1.329 Å, r(C=S) = 1.597 Å, r(C–Cl) = 1.724 Å, ∠(FCS) = 124.0°, ∠(ClCS) = 127.2° (calc) [2] r(C–F) = 1.339 Å, r(C=S) = 1.593 Å, r(C–Cl) = 1.718 Å, ∠(FCS) = 123.6°, ∠(ClCS) = 127.3° (expt) [71]	
FBrCZ	r(C–F) = 1.294 Å, r(C=S) = 1.585 Å, r(C–Br) = 1.887 Å, ∠(FCS) = 124.0°, ∠(BrCS) = 126.9° (calc) [2] r(C–F) = 1.330 Å, r(C=S) = 1.595 Å, r(C–Br) = 1.901 Å, ∠(FCS) = 124.4°, ∠(BrCS) = 127.2° (calc) [2]	
ClBrCZ	r(C–Cl) = 1.725 Å, r(C=S) = 1.586 Å, r(C–Br) = 1.898 Å, ∠(ClCS) = 124.1°, ∠(BrCS) = 123.9° (calc) [2] r(C–Cl) = 1.733 Å, r(C=S) = 1.602 Å, r(C–Br) = 1.915 Å, ∠(ClCS) = 124.6, ∠(BrCS) = 124.0° (calc) [2]	

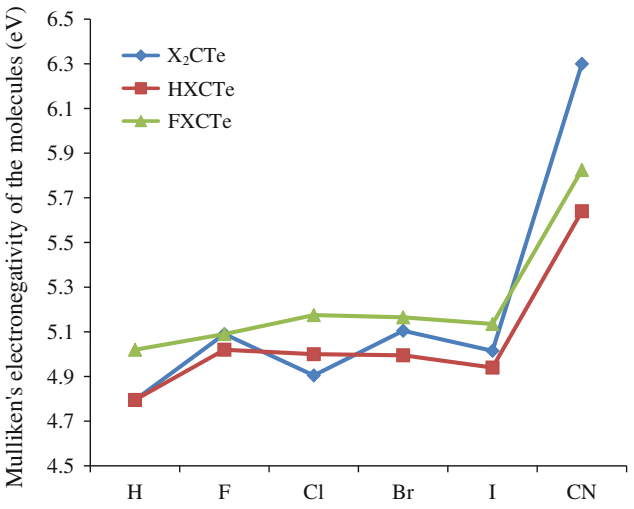

Fig. 21 Mulliken's electronegativity of the X_2CTe, HXCTe and FXCTe molecules upon replacement of substituent (X)

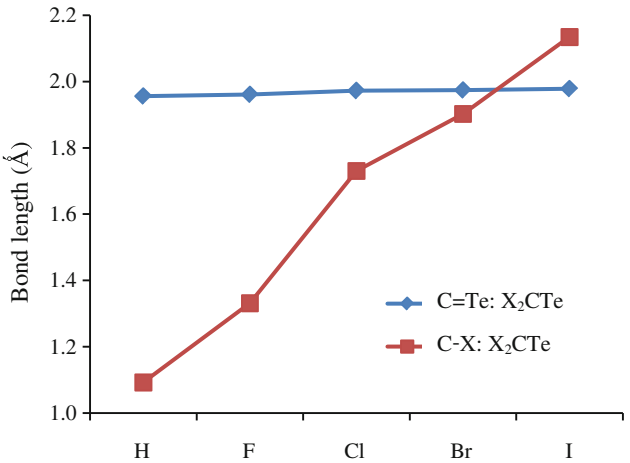

Fig. 22 The C=Te and C–X bond lengths (Å) (MP2) of the X_2CTe species as a function of halogen substituent

The highest ionization potential of the species occurs where X or Y = CN and/or F can also be correlated with the ionic character of the carbonyl compounds. The electronegative substituent, X or/and Y, withdraws electron density from the carbonyl center, weakening the σ C–F bond; thus, the π donation from the tellurium atom is increased. The atomic charges on the carbonyl carbon and

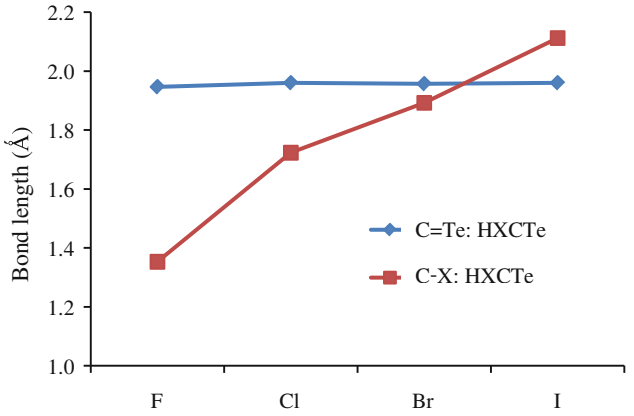

Fig. 23 The C=Te and C–X bond lengths (Å) (MP2) of the HXCTe species as a function of halogen substituent

the tellurium atom decrease. The decrease in ionization potentials with respect to the X or Y substituent from CN to I is consistent with the changes observed in the charge on the carbonyl carbon as illustrated in Fig. 24. The linear correlation between the substituent X and/or Y with the energy differences between the neutral and the corresponding cationic species is presented in Fig. 25. The changes observed in the charge on the carbonyl carbon of the telluroformaldehyde derivatives studied are directly proportional to the trend observed in the predicted ionization potentials. The ionization potentials can be rationalized in terms of the charge on the carbonyl carbon, as well as the electronegativity of the substituent or ligand (X and/or Y) directly bonded to the carbonyl center. Hence, the net charge, σ-donation and backbonding of both the substituent and the chalcogen are the factors affecting the ionization potential of the X_2CTe and XYCTe species, synergistically.

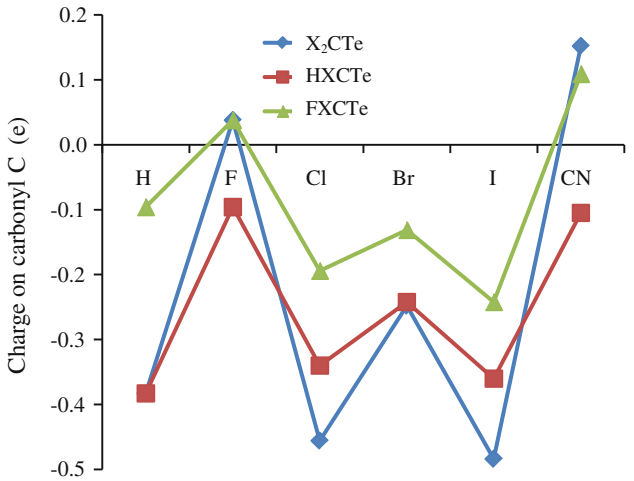

Fig. 24 Trend in the charge (e) (MP2) on the carbonyl carbon upon substituent (X) replacement for the X_2CTe, HXCTe and FXCTe species

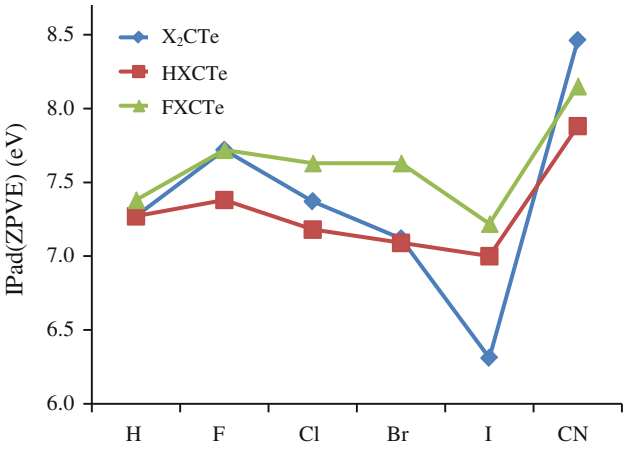

Fig. 25 Adiabatic ionization potentials, $IP_{ad(ZPVE)}$, (eV) (MP2) versus the substituents

The experimentally obtained ionization potentials of H_2CZ (Z = O, S, Se) are reported to be 10.88 [9], 9.44 [19] and 8.80 [31] eV, respectively, and these are also included in Table 6. The shift in the ionization potential from formaldehyde to thioformaldehyde, selenoformaldehyde and telluroformaldehyde are +1.44, +2.08 and +3.60 eV, respectively. Substituting the oxygen in formaldehyde by sulfur, selenium or tellurium increases the chalcogen character of the molecule, which in turn increases the shift in the ionization potential significantly [54]. This is in agreement with the systematic decrease observed in the first ionization potential of the H_2CX (X = O, S, Se and Te) molecules.

4.3 Electron affinities

With increasing halogen atom size, a gradual increase in the electron affinities of the X_2CTe and XYCTe species is noted. The linear correlation between the Pauling electronegativities of the halogens and the cyano-group with the energy differences between the neutral and the corresponding anionic species is depicted in Fig. 26. Since the presence of a strongly electron-withdrawing substituent directly attached to the carbonyl center reduces the population of the $2s$ and $2p$ orbitals of carbon, an abrupt decrease in electron affinity from H to F could conceivably be expected. However, the contrary is observed in this research. This shows that there is some shielding effect from the lone pairs of tellurium acting against the decrease in the electron affinities of the fluoro-telluroformaldehyde derivatives. The presence of the conjugation by the heteroatom lone pairs provides strong π donor character. The electronegative substituent, X and/or Y, withdraws electron density from the carbonyl center, increasing the charge, which in turn makes the carbon a better π acceptor and enhances π donation from the chalcogen. Thus, the polarity

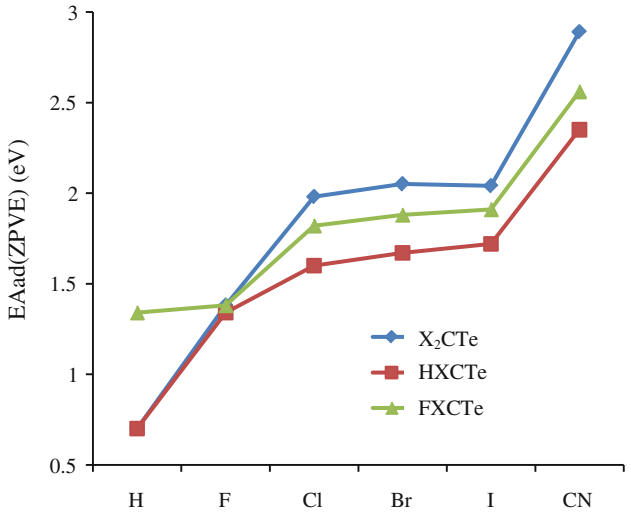

Fig. 26 Adiabatic electron affinities, $EA_{ad(ZPVE)}$, (eV) (MP2) versus the substituents

is reversed, and the carbon atom is significantly negative relative to the tellurium atom. The linear correlation of the halogen Pauling electronegativities with the electron affinities can be explained as a result of the decreasing order of electron-withdrawing ability of the halogen X or Y and the decreasing back donation from the tellurium atom. This is in agreement with the trends observed in Figs. 24, 26 for the halogen derivatives only.

Moreover, for X or Y = F ($\chi_F = 3.98$), the lone pair of the fluorine substituent crowds into the π orbital of the carbonyl carbon, creating a shielding effect which also acts against the decrease in the electron affinities. It is also predicted that the sp^2 hybridization is reduced down the halogen group. Thus, the stabilization of the σ-nonbonding orbital by electron-withdrawing substituents such as halogen increases the 2*s* character of the carbonyl carbon. The 2*p* contribution to the σ C–F bond is higher in the singlet state than in the corresponding triplet state, which agrees well with the longer C–F bond distance of the latter. Hence, the electronegativities of the substituents are not the sole factor in determining the ability of these species to accept an additional electron. This electron capturing ability is dependent on the substituent X or Y and the polarity of the C=Te bond.

The experimental adiabatic electron affinity of formaldehyde and thioformaldehyde is −0.65 [7] and 0.47 [21] eV, respectively. To our knowledge, the electron affinity of selenoformaldehyde has not been reported yet. In a crude picture, the electron affinity can be related to the orbital energy of the LUMO by Koopmans' theorem [55]. Moreover, it is reported that there is a significant lowering of the orbital energy for the π^* LUMO of these carbonyls, on changing O in formaldehyde to S and a moderate lowering on changing S to Se or Te [56]. Since the energy level of the π^* orbital is lowered, the addition of an extra electron is facilitated, which in turn agrees with the positive electron affinities of thioformaldehyde and telluroformaldehyde. Therefore, moving down the H_2CZ (Z = O, S, Se and Te) carbonyl series, the anionic form is lowered in energy compared to the neutral molecule.

4.4 Singlet–triplet splittings

Table 5 reports the singlet–triplet splittings for all the molecules studied in this research. The trend is appreciable; the largest singlet–triplet gap appears where the fluoro substituent is attached to the carbonyl carbon center, and the splitting decreases on approaching the iodo-telluroformaldehyde derivatives. Hydrogen is less electronegative than iodine, resulting in the lowest singlet–triplet gap for the X or Y = H species. The presence of a strongly electronegative substituent stabilizes the $^1A'$ singlet state, and the $^3A''$ state energy lies higher. In the lowest singlet state, the a′ symmetry molecular orbital is the HOMO, a σ-type nonbonding orbital having contributions from the in-plane *p* orbitals of the carbonyl carbon, the substituent X = F, Cl, Br, I and CN. The effect of the electronegativity and the size of the halo substituents are reflected in the HOMO energies. The participation of the carbon *s* orbital in the bonding is expected to be large in the case of the fluoro-telluroformaldehyde derivatives as fluorine is the most electronegative ($\chi_F = 3.98$) halogen. This leads to an increase in the HOMO–LUMO gap (E_{H-L}) favoring the singlet state. Figure 27 illustrates the substituent replacement effect on the HOMO–LUMO gap of the X_2CTe and the XYCTe species (X,Y = H, F, Cl, Br, I and CN). The a″ orbital is the LUMO in the singlet becomes the SOMO for the corresponding triplet state. Fluorination results in the highest value of the E_{H-L}, and consequently, this is reflected in the predicted singlet–triplet splittings. Figure 28 displays the singlet–triplet gaps (eV) as a function of halogen substituent. As the electronegativity of the substituent decreases from fluorine to iodine, the energy of the a′ HOMO is raised. In the triplet species with a decrease in the electronegativity and an increase in the size of the substituent, the antibonding character of the a″ orbital is decreased and the orbital energy is lowered. Thus, on going down the halogen group, the a′ and a″ orbital energy separation tends to decrease. Figure 29 depicts the link between the HOMO–LUMO gaps and the singlet–triplet splittings of X_2CTe, HXCTe and FXCTe species, good linear correlation observed ($R^2 = 0.893$).

The maximum hardness principle states that there seems to be a rule of nature that molecules arrange themselves so as to be as hard as possible [73]. Hardness is interrelated to

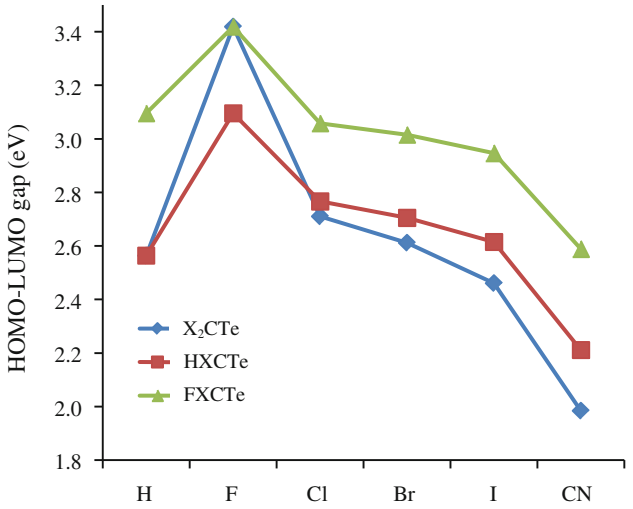

Fig. 27 HOMO–LUMO gap (eV) (B3LYP) as a function of the substituents

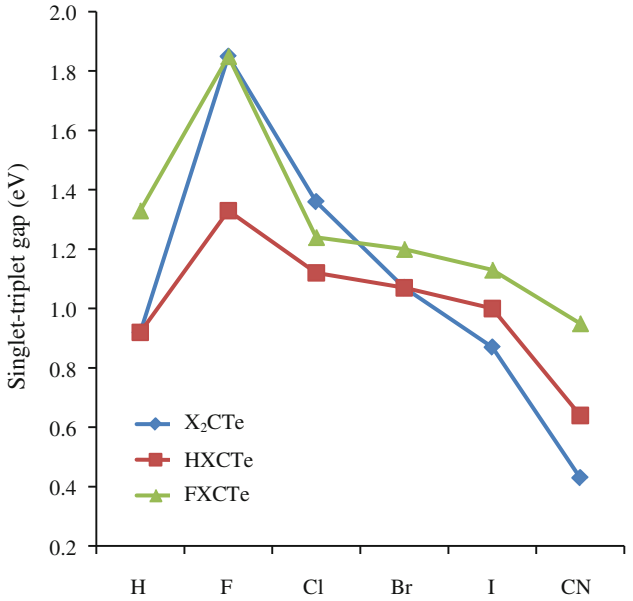

Fig. 28 Graph of singlet–triplet splittings (eV) (B3LYP) versus the substituents

the energy gap between the two frontier orbitals [74]. The relationship between hardness and HOMO–LUMO gap is given by: $\eta = (E_{LUMO} - E_{HOMO})/2$ [75]. Hardness of the X_2CTe and XYCTe species ranges from 0.99 ($(NC)_2CTe$) to 1.71 eV (F_2CTe). A hard molecule has a large HOMO–LUMO gap, and a soft molecule has a small HOMO–LUMO gap [74]. Thus, the $X_2C{=}Te$ and XYC=Te families can be classified as soft chemical species, which in turn predicts their high reactivities and low stabilities. Since ΔE_{H-L} is found to be proportional to ΔE_{S-T}, hardness can also be related to the singlet–triplet separation, good linear correlation obtained ($R^2 = 0.894$).

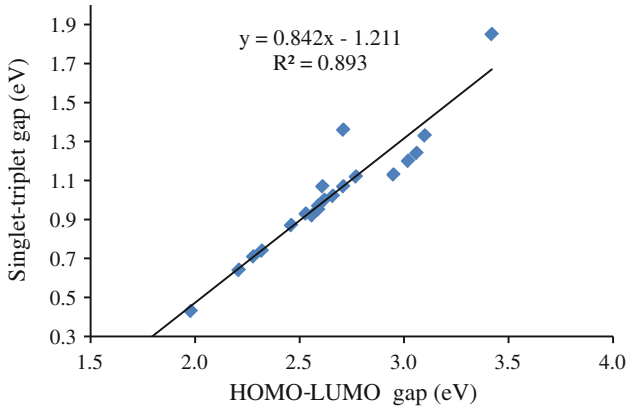

Fig. 29 Linear correlation between HOMO–LUMO gap and singlet–triplet splittings (eV) (B3LYP) versus the substituents

The Mulliken's atomic charge on the carbon atom is significantly negative relative to the Te atom. The charges on the carbonyl carbon for these species decrease on halogeno-substitution in the order F > Cl > Br > I > H as shown in Fig. 21. The 2*s* and 2*p* populations on the carbon center are the smallest when a strongly electron-withdrawing substituent is directly attached. The σ orbitals of the carbon–halogen bonds have some antibonding character. The 2*s* carbon contribution to the sp^2 hybridization strongly decreases in going from fluorine to iodine.

The predicted singlet–triplet separations can be rationalized in terms of the charge on the carbonyl carbon, and the electronegativity of the substituent directly bonded to the carbonyl center. Hence, the net charge, σ-donation and π back bonding help provide an understanding of the singlet–triplet splittings.

5 Conclusions

The structural parameters, ionization potentials and four different neutral–anion energy differences (namely, EA_{ad}, $EA_{ad(ZPVE)}$, VEA and VDE) as well as the singlet–triplet splittings of the X_2CTe and XYCTe species (X,Y = H, F, Cl, Br, I and CN) have been predicted here. To our knowledge, the present findings for telluroformaldehyde and its derivatives are reported for the first time. The predicted values for the ZPVE adiabatic ionization potential of the X_2CTe species range from 6.31 [I_2CTe] to 8.26 [$(NC)_2CTe$] eV and the $EA_{ad(ZPVE)}$ values range from 0.70 [H_2CTe] to 2.89 [$(NC)_2CTe$] eV (MP2). For the XYCTe species, the $IP_{ad(ZPVE)}$ range from 7.00 [HICTe] to 8.15 [Br(NC)CTe] and the $EA_{ad(ZPVE)}$ values range from 1.34 [HFCTe] to 2.70 [$(CN)_2CTe$] eV (MP2). The energetic of the telluroformaldehyde derivatives may be rationalized in terms of the electronegativity of the halogen or ligand directly bonded to the carbon, the partial charge on the carbonyl carbon and

tellurium atom and the σ-donation and π backbonding of the substituent and the chalcogen. On comparing the first ionization potential and the electron affinity of the H_2CX (X = O, S Se and Te) carbonyls, it is noted that there is a great dependence on the chalcogen. The HOMO–LUMO separations are small, within the range of 1.98–3.10 eV, suggesting the existence of a rich spectrum for X_2CTe and XYCTe compounds in the visible regions. The results obtained from the MP2 and DFT computations are usually in good agreement. However, MP2 singlet–triplet separations are not reliable, since MP2 artificially favors the triplet states. We suggest that these computations furnish reliable information for the species studied in this research. Since experimental data are still lacking, this work should assist experimental studies on organotellurium chemistry in the future.

Acknowledgments The research has been supported by the Mauritius Tertiary Education Commission (TEC). We acknowledge the use of the facilities at the University of Mauritius, the School of Chemical Sciences, Universiti Sains Malaysia, Penang, Malaysia, and the Center for Computational Quantum Chemistry (CCQC) at the University of Georgia. The authors are grateful to the anonymous reviewers for their help in improving the manuscript. This paper is dedicated to Professor E. D. Jemmis: gentleman, friend and uniquely gifted scholar.

References

1. Kwiatkowski JS, Leszczyski J (1994) Mol Phys 81:119–131
2. Kwiatkowski JS, Leszczyski J (1993) Mol Phys 97:1845–1849
3. Liao HY, Su MD, Chu SY (2000) J Chem Phys 261:275–287
4. Melnick JG, Yurkerwich K, Parkin G (2010) J Am Chem Soc 132:647–655
5. Butler R, Snelson A (1979) J Phys Chem 83:3243–3248
6. Rinsland CP, Zander R, Brown LR, Farmer CB, Park JH, Norton RH, Russel JM, Raper OF (1986) Geophys Res Lett 13:769–772
7. Burrow PD, Michejda AJ (1976) Chem Phys Lett 42:223–236
8. Gray SK, Miller WH, Yamaguchi Y, Schaefer HF (1981) J Am Chem Soc 103:1900–1904
9. Ohno K, Okamur K, Yamakado H, Hoshino S, Takami T, Yamauchi M (1995) J Phys Chem 99:14247–14253
10. Francisco JS, Thoman JW (1999) Chem Phys Lett 300:553–560
11. Lai C-H, Su M-D, Chu S-Y (2001) J Chem Phys 105:6932–6937
12. Zhao Y, Francisco JS (1992) Mol Phys 77:1187–1195
13. Francisco JS, Li Z (1989) J Phys Chem 93:8118–8122
14. Chestnut DB, Phung CG (1989) J Chem Phys 91:6238–6244
15. Francisco JS, Ostafin A (1989) Mol Phys 68:255–260
16. Dixon DA, Farnham WB, Smart BE (1990) Inorg Chem 29:3954–3960
17. Francisco JS, Zhao Y (1992) J Chem Phys 96:7587–7596
18. Francisco JS (1992) J Chem Phys 96:7597–7602
19. Jones A, Lossing FP (1967) J Phys Chem 71:4111–4113
20. Collins S, Back TG, Rauk A (1993) J Am Chem Soc 107:6589–6592
21. Staneke PO, Groothuis G, Ingemann S, Nibbering NMM (1995) Int J Mass Spectrom Ion Processes 149:99–110
22. See-Wing C, Wai-Kee L, Weh-Bih T, Cheuk-Yiu N (1992) J Chem Phys 97:6557–6568
23. Brunton L, Chabner B, Knollman B (2010) The pharmacological basis of therapeutics. Mc Graw-Hill Professional, New York
24. Kirschner S, Wei YK, Francis D, Bergman JG (1969) J Med Chem 9:369–372
25. Careless AJ, Kroto HW, Landersberg BM (1973) J Chem Phys 1:371–375
26. Nakata M, Fukuyama T, Kuchitsu K (1982) J Mol Struct 81:121–129
27. Duncan JL (1978) Mol Phys 28:1177–1191
28. Fabricant B, Krieger D, Muenter JS (1977) J Chem Phys 67:1576–1579
29. Winnerwisser G, Cornet RA, Birss FW, Gordon RM, Ramsay DA, Till SM (1979) J Mol Spectrosc 74:327–330
30. Brown RD, Godfrey PD, McNaughton D (1985) Chem Phys Lett 118:29–31
31. Bock H, Aygen S, Rosmus P, Solouki B, Weissflog E (1984) Chem Ber 117:187–202
32. Jansson E, Norman P, Minaeve B, Agren H (2006) J Phys Chem 124:114016–114020
33. Roper WR, Headford CEL (1983) J Organomet Chem 244:C53–C56
34. Roper WR, Hill AF, Waters JM, Wright AH (1983) J Am Chem Soc 105:5939–5940
35. Tokitoh N (1998) Phosphorus Sulphur and Silicon 123:136–138
36. Matsumoto T, Tokitoh N, Okazaki R (1999) J Am Chem Soc 121:8811–8824
37. Iwamoto T, Sato K, Ishida S, Kabuto C, Kira M (2006) J Am Chem Soc 128:16914–16920
38. Panda A (2009) Coord Chem Rev 253:1947–1965
39. Møller C, Plesset MS (1934) Phys Rev 46:618–622
40. Frisch MJ, Trucks GW, Schlegel HB, Scuseria GE, Kudin KN, Burant JC, Millam JM, Iyengar SS, Tomasi J, Robb MA, Cheeseman JR, Montgomery JA, Vreven T, Barone V, Mennucci B, Cossi M, Scalmani G, Rega N, Petersson GA, Nakatsuji H, Hada M, Ehara M, Toyota K, Fukuda R, Hasegawa J, Ishida M, Nakajima T, Honda Y, Kitao O, Nakai H, Klene M, Li X, Knox JE, Hratchian HP, Cross JB, Adamo C, Jaramillo J, Gomperts R, Stratmann RE, Yazyev O, Austin AJ, Cammi R, Pomelli C, Ochterski JW, Ayala PY, Morokuma K, Voth GA, Salvador P, Dannenberg JJ, Zakrzewski VG, Dapprich S, Daniels AD, Strain MC, Farkas O, Malick DK, Rabuck AD, Raghavachari K, Foresman JB, Ortiz JV, Cui Q, Baboul AG, Clifford S, Cioslowski J, Stefanov BB, Liu G, Liashenko A, Piskorz P, Komaromi I, Martin RL, Fox DJ, Keith T, Al-Laham MA, Peng CY, Nanayakkara A, Challacombe M, Gill PMW, Johnson B, Chen W, Wong MW, Gonzalez C, Pople JA (2004) Gaussian 03 Revision C 02. Gaussian Inc, Wallingford CT
41. Becke AD (1988) J Chem Phys 38:3098–3100
42. Becke AD (1993) J Chem Phys 98:1372–1377
43. Lee C, Yang W, Parr RG (1988) Phys Rev B 37:785–789
44. Hay PJ, Wadt WR (1985) J Chem Phys 82:270–283
45. Hay PJ, Wadt WR (1985) J Chem Phys 82:284–298
46. Hay PJ, Wadt WR (1985) J Chem Phys 82:299–310
47. Glukhovstev MN, Pross A, McGrath MP, Radom L (1995) J Chem Phys 103:1878–1885
48. Huzinaga S (1965) J Chem Phys 42:1293–1302
49. Dunning TH, Hay PJ (1977) In Modern Theoretical Chemistry Schaefer H F Ed Plenum New York 3:1–28
50. Huzinaga S (1971) Approximate Atomic Wavefunctions II. University of Alberta, Edmonton Alberta
51. Schafer A, Horn H, Ahlrichs R (1992) J Chem Phys 97:2571–2577
52. Lee TJ, Schaefer HF (1985) J Chem Phys 83:1784–1794
53. Alfred AL (1961) J Inorg Nucl Chem 17:215–221
54. Glass RS, Gruhn EN, Lichtenberger DL, Lorance E, Pollard RJ, Birringer M, Block E, Deorazio R, He C, Shan Z, Zhang X (2000) J Am Chem Soc 122:5065–5074
55. Koopmans TA (1933) Physica 1:104–113

56. Orlova G, Goddard JD (2001) J Org Chem 66:4026–4036
57. Carpenter JH (1974) J Mol Spectrosc 50:182–201
58. Buckley TJ, Johnson RD, Huie RE, Zhang Z, Kuo SC, Klemm RB (1995) J Phys Chem 99:4879–4885
59. Carpenter JH, Rimmer DF (1978) J Chem Soc Faraday Trans 74:466–476
60. Johnson KM, Powis I, Danby C (1979) J Int J Mass Spectrom Ion Phys 32:1–14
61. Carpenter JH, Smith JG, Thompson IH, Whiffen DH (1977) J Chem Soc Faraday Trans 73:384–393
62. Thomas RK, Thompson H (1972) Proc R Soc London A 327:13–22
63. Johnson DR, Powell FX, Kirchoff WH (1971) J Mol Spectrosc 39:136–145
64. Beers Y, Klein GP, Kirchoff WH, Johnson DR (1972) J Mol Spectrosc 44:533–535
65. Binnewies M, Grosse J, Le Van D (1985) Phosphorus Sulfur 21:349–366
66. Hildenbrand DL (1973) J Phys Chem 77:897–917
67. Mines GW, Thomas RK, Thompson H (1973) Proc R Soc London A 333:171–181
68. Wittel K, Hass A, Bock H (1972) Chem Ber 105:3865–3868
69. Brown RD, Godfrey PD, McNaughton D, Taylor PR (1986) J Mol Spectrosc 120:292–297
70. Christen D, Oberhammer H, Zeil W, Haas A, Darmadi A (1980) J Mol Struct 66:203–210
71. Gleisberg F, Haberl A, Zeil WZ (1975) Naturforsch 30A:549–558
72. Parr RG, Donnelly RA, Levy M, Palke WE (1978) J Chem Phys 117:3801–3807
73. Parr RG, Chattaraj PK (1991) J Am Chem Soc 113:1854–1855
74. Pearson RG (2005) J Chem Sci 117:369–377
75. Priyakumar UD, Sastry GN (2002) J Org Chem 67:271–281